ADAR1 Regulates Lipid Remodeling to Dictate Ferroptosis Sensitivity

Che-Pei Kung[1], Nick D. Terzich[2], Ma Xenia G. Ilagan[3,4], Michael J. Prinsen[3,4], Madhurima Kaushal[5], Raleigh D. Kladney[1], Jade H. Weber[1], Alex R. Mabry[1,6], Luisangely Soto Torres[1,6], Emily R. Bramel[1], Eric C. Freeman[1], Thwisha Sabloak[1], Sua Ryu[1], William M. Weber[1], Kyle A. Cottrell[7], Leonard B. Maggi Jr.[1], Leah P. Shriver[2,8,9], Gary J. Patti[2,10,11] and Jason D. Weber[1,11,12,13]

[1]Department of Medicine, Division of Molecular Oncology, Washington University School of Medicine, Saint Louis, MO, USA

[2]Department of Chemistry, Washington University, St. Louis, MO, USA

[3]High Throughput Screening Center, Washington University School of Medicine, Saint Louis, MO, USA

[4]Department of Biochemistry and Molecular Biophysics, Washington University School of Medicine, Saint Louis, MO, USA

[5]Institute for Informatics, Data Science and Biostatistics, Washington University School of Medicine, Saint Louis, MO, USA

[6]Cancer Biology Graduate Program, Washington University School of Medicine, Saint Louis, MO, USA

[7]Department of Biochemistry, Purdue University, West Lafayette, IN, USA

[8]Department of Medicine, Division of Nutritional Science and Obesity Medicine, Washington University School of Medicine, Saint Louis, MO, USA

[9]Center for Mass Spectrometry and Metabolic Tracing, Washington University, St. Louis, MO, USA

[10]Department of Genetics, Washington University, St. Louis, MO, USA

[11]Siteman Cancer Center, Washington University, St. Louis, MO, USA

[12]Department of Cell Biology and Physiology, Washington University School of Medicine, Saint Louis, MO, USA

[13]Department of Biology, Washington University, Saint Louis, MO, USA

Co-correspondence:
Che-Pei Kung, Ph.D.
Department of Medicine, Division of Molecular Oncology

Washington University School of Medicine
660 South Euclid Avenue
Campus Box 8069
St. Louis, MO 63110 USA
Email: patkung@wustl.edu
Telephone: 314-747-3898
Fax: 314-362-0152

and

Jason D. Weber, Ph.D.
Department of Medicine, Division of Molecular Oncology
Department of Cell Biology and Physiology

Washington University School of Medicine
660 South Euclid Avenue
Campus Box 8069
St. Louis, MO 63110 USA
Email: jweber@wustl.edu
Telephone: 314-747-3896
Fax: 314-362-0152

Summary

Triple-negative breast cancer (TNBC), defined by the lack of estrogen, progesterone, and HER2 receptor expressions, is aggressive and lacks targeted treatment options. Adenosine deaminase acting on RNA 1 (ADAR1) has been shown to contribute to TNBC tumorigenesis by modulating an innate immune response. However, little is known about its role in the regulation of metabolic fitness of TNBC. We tested the hypothesis that ferroptosis is an ADAR1-protected vulnerability by showing that ADAR1 knockdown sensitizes TNBC cells to ferroptosis inducers. Lipidomic analyses showed that ADAR1 loss increased the abundance of phospholipids enriched with polyunsaturated fatty acids (PUFA), of which peroxidation is the main driver of ferroptosis. Transcriptomic analyses discovered that the proto-oncogene MDM2 contributes to the lipid remodeling phenotype. A ferroptosis-focused drug screen identified FDA-approved cobimetinib as a drug-repurposing candidate to synergize with ADAR1 loss. This finding supports further basic, pre-clinical, and clinical studies to develop novel therapeutic strategies for TNBC through ADAR1-mediated metabolic regulation.

Keywords: ADAR1, RNA editing, TNBC, ferroptosis, RSL3, lipid remodeling, PUFA, MUFA, MDM2, cobimetinib.

Introduction

Despite the recent development of PARP inhibitors, immunotherapy, and antibody-drug conjugates, there remains a significant gap in targeted therapies for TNBC, contributing to its poor prognosis[1]. A multi-prong approach is underway to investigate the immunogenic, epigenetic, and metabolic landscapes of TNBC to identify points of vulnerability[2-4].

One such vulnerability is ferroptosis, a distinctive form of programmed cell death that depends on iron-mediated peroxidation of long polyunsaturated fatty acids (PUFA) to break down cell membranes[5]. Compared to other BC subtypes, TNBC cells express lower levels of iron exporter ferroportin, resulting in an increase in labile iron pools[6]. TNBC cells have also been shown to increase the uptake of cystine, a precursor for the antioxidant glutathione, rendering them more vulnerable to inhibitions of the glutamate/cystine antiporter xCT and glutathione effector GPX4[7,8]. TNBC's sensitivity to ferroptosis is also correlated with abundance of PUFA, regulated by enzymes contributing to PUFA biosynthesis, such as Acyl-CoA synthetase long-chain family member 1 and 4 (ACSL1/4), as well as fatty acid desaturases 1 and 2 (FADS1/2)[9-11].

Adenosine deaminase acting on RNA 1 (ADAR1, encoded by *ADAR*) converts adenosine to inosine within cellular dsRNA, in a process known as A-to-I editing. Elevated expression of ADAR1 is prevalent in breast cancer, and ADAR1-mediated editing contributes to tumor progression and resistance to therapy in breast cancer, including TNBC[12,13]. We have previously reported a TNBC-centric ADAR1 dependency phenomenon, in which ADAR1 protects TNBC cells from translational stress and type I interferon activation predisposed by elevated levels of interferon stimulated gene signatures[14]. ADAR1-mediated regulation of the innate immune response has been observed in several types of cancer, and the loss of ADAR1 has been shown to

98 sensitize certain cancers to immunotherapy[15-18]. Through its ability to prevent the cytotoxic
99 inflammatory response, ADAR1 also protects cancer cells from other anti-tumorigenic stresses,
100 such as necroptosis and epigenetic modulation[19,20]. However, few studies have investigated the
101 ability of ADAR1 to regulate the metabolic fitness of cancer cells and their sensitivity to
102 metabolic stress. Considering the role of ADAR1 in metabolic regulation and the importance of
103 cancer metabolism, it is important to fill these knowledge gaps[21,22].

104 In the current study, we demonstrate that ADAR1 protects TNBC cells from ferroptosis by
105 regulating the expression of MDM2 and lipid profiles. Our observations indicate broader
106 applications of ADAR1-targeting therapies against TNBC.

107 **Results**

108 **ADAR1 protects TNBC cells from ferroptosis induction**

109 To determine whether ADAR1 inhibits ferroptosis directly, ADAR1 was knocked down with a
110 short hairpin RNA (shRNA) in the TNBC cell line MDA-MB-231 (**Figure S1A**). The level of
111 malondialdehyde (MDA), a byproduct and marker of lipid peroxidation, was measured to show
112 that cells with ADAR1 knockdown (ADAR1-deficient) did not display induced ferroptosis
113 phenotype compared to ADAR1-intact cells treated with a non-targeting shRNA (shNT) (**Figure**
114 **S1B**). Similarly, by staining for both the reduced and oxidized forms of the lipid peroxidation
115 probe BODIPY™ 581/591 C11, it was revealed that ADAR1 knockdown did not improve the
116 cells' ability to oxidize PUFA (**Figure S1C-D**). Cell viability assay was performed to show that
117 reduced proliferation and viability of MDA-MB-231 cells resulting from ADAR1 knockdown
118 could be partially rescued by an apoptosis inhibitor (Z-VAD-FMK) or an eIF2α inhibitor

119 (ISRIB), but not by ferroptosis inhibitors Ferrostatin-1 or Liproxstatin-1 (**Figure S1E**). These
120 results suggest that the reduction of ADAR1 does not overtly induce ferroptosis phenotypes.

121 ADAR1-intact and -deficient MDA-MB-231 cells were then tested to determine whether
122 ADAR1 expression influences the sensitivity of cells to ferroptosis induction. Ferroptosis can be
123 induced by the GPX4 inhibitor RSL3, whose effect can be rescued by the ferroptosis inhibitors
124 Ferrostatin-1 or UAMC, but not Z-VAD-FMK or necroptosis inhibitor Necrostatin-1 (**Figure**
125 **S1F**). ADAR1-deficient cells were found to be more sensitive to RSL3 at concentrations as low
126 as 50nM (**Figure 1A**). Cell viability assay was performed to determine the IC_{50} (half-maximum
127 inhibitory concentration) of RSL3, and ADAR1-deficient cells (IC_{50} = 0.11μM vs 2.9μM) were
128 27 times more sensitive compared to ADAR1-intact cells (**Figure 1B**). A similar level of
129 sensitization was observed when using another GPX4 inhibitor, ML162 (IC_{50} = 0.08μM vs
130 2.27μM) (**Figure 1C**).

131 To evaluate whether this sensitization effect occurs in TNBC cells in addition to MDA-MB-231,
132 multiple TNBC cell lines (MDA-MB-436, HCC1806, MDA-MB-468, BT20, BT549) were
133 tested. In all TNBC cell lines tested, ADAR1 knockdown resulted in increased RSL3 sensitivity,
134 ranging from 1.8-fold (BT549) to 9.8-fold (MDA-MB-436) (**Figure 1D-F, Figure S1G-H**).
135 Multiple non-TNBC cell lines (MCF7, T47D, BT474, SKBR3, MDA-MB-361, ZR75.1) were
136 also tested. Interestingly, by arbitrarily setting IC_{50}shNT/IC_{50}shADAR1=1.5 as the threshold for
137 sensitization, none of the non-TNBC cell lines acquired higher sensitivity after ADAR1
138 knockdown (**Figure 1G-J, Figure S1I-K**). A cell line derived from a TNBC PDX (patient-
139 derived xenograft), WHIM12, was also shown to be highly sensitized to RSL3 after ADAR1
140 knockdown (**Figure 1K**). These results indicate that ADAR1 protects TNBC, but not non-
141 TNBC, cell lines from ferroptosis induction.

142 An orthotopic implantation mouse model was established to test whether these *in vitro* results
143 can be recapitulated *in vivo*. MDA-MB-231 cells stably transduced with Tet-inducible shADAR1
144 were implanted in the mammary fat pad of female immunocompromised NSG mice (**Figure 2A-**
145 **B**). Upon the formation of palpable tumors, half of the mice were switched to a diet containing
146 doxycycline to induce ADAR1 knockdown (**Figure S2A**). Both control and doxycycline diet
147 mice were subjected to intraperitoneal (i.p.) injection of RSL3 (100mg/kg weight; twice a week)
148 for 5 weeks. Weekly health and weight monitoring did not suggest additional toxicity associated
149 with RSL3 treatment (**Figure S2B**). Doxycycline diet or RSL3 treatment alone reduced tumor
150 burdens, and mice that received both experienced significantly slower tumor progression (**Figure**
151 **1C-E, Figure S2C-E**). Immunohistochemical (IHC) staining of ADAR1 in resected tumors
152 confirmed a sustained overall reduction in ADAR1 expression (**Figure 2F and S2F**). IHC
153 staining of 4-Hydroxynonenal (4HNE), a product of lipid peroxidation, showed that the
154 combination treatment enhanced the ferroptosis phenotype (**Figure 2F-G**). Moreover, showing a
155 mosaic pattern of staining in doxycycline/RSL3-treated tumors, ADAR1 levels can be seen to be
156 inversely correlated with 4HNE staining (**Figure S2G**). Together, these results suggest that
157 ADAR1 reduction also sensitizes cancer cells to ferroptosis induction to suppress tumor
158 progression *in vivo*.

159 **Knockdown of ADAR1 leads to lipid remodeling**

160 Multiple factors contribute to ferroptosis sensitivity, including ferrous iron availability,
161 glutathione activity, and the relative abundance of PUFA over monounsaturated fatty acid
162 (MUFA)[5] (**Figure 3A**). To test the hypothesis that ADAR1-deficient cells are primed for
163 ferroptosis induction, these elements were evaluated using the MDA-MB-231 cell line, as it is
164 highly sensitive to ferroptosis induction by ADAR1 knockdown.

165 In ADAR1-deficient cells, both the level of total glutathione and the ratio between reduced and
166 total glutathione were unchanged (**Figure S3A-B**). FerroOrange staining was used to show that
167 ADAR1-deficient cells do not display significantly higher levels of ferrous iron (**Figure S3C-D**).
168 This suggests that elevated sensitivity to ferroptosis after ADAR1 knockdown cannot be
169 attributed to altered glutathione activity or the abundance of ferrous iron.

170 Consequently, a targeted lipidomic analysis was performed to identify possible changes in lipid
171 profiles after ADAR1 knockdown. Interestingly, a clear pattern change was detected with the
172 phosphatidylcholine (PC) species, the most abundant phospholipid in mammalian cells and the
173 most impactful phospholipid in controlling sensitivity to ferroptosis (**Figure 3B**). The observed
174 lipid reprogramming disproportionally enriched PC species with longer carbon chains and higher
175 degrees of unsaturation (**Figure 3C-F**). Some of the longest and most highly unsaturated PC
176 species, such as PC38:4, are among the most significantly enriched PCs in ADAR1-deficient
177 cells (**Figure 3G, Figure S3E**).

178 To investigate whether similar lipid reprogramming occurs in TNBC cells sensitized to ADAR1
179 knockdown to a lesser extent, lipidomic analysis was performed with ADAR1-deficient MDA-
180 MB-436 cells (**Figure S3F**). Several highly unsaturated PCs, such as PC 34:3, 35:3, and 44:6,
181 were enriched after ADAR1 knockdown (**Figure S3G-I**). However, enrichment was not limited
182 to PUFA, as some MUFA PC species (i.e. PC36:1, 37:1, 38:1) were also upregulated. Some
183 PUFA PC species appeared to be reduced (**Figure S3G**).

184 Interestingly, PUFAs from other phospholipid families, such as phosphatidylserine (PS) and
185 phosphatidylethanolamine (PE), were also enriched in ADAR1-deficient MDA-MB-436 cells
186 (**Figure S3J-N**). These results showed that the reduction of ADAR1 leads to lipid remodeling,

187 specifically enrichment of PUFA over MUFA and saturated fatty acid (SFA). The publicly
188 available metabolomics dataset shows that ADAR1 expression levels were strongly correlated
189 with the abundance of SFA (PC32:0) and MUFA (PC32:1 and PC34:1) species in TNBC, but not
190 non-TNBC cells (**Figure 3H-J**). These data support the hypothesis that in TNBC cells, ADAR1
191 helps maintain FA homeostasis to protect cells from ferroptosis.

192 **ADAR1 regulates MDM2 expression to dictate lipid profiles and ferroptosis sensitivity**

193 To identify mechanisms contributing to ADAR1-regulated lipid remodeling, four TNBC cell
194 lines, including those that are more highly (>5-fold - MDA-MB-231, MDA-MB-468) or
195 moderately (<5-fold - HCC1806, BT549) sensitized to RSL3 after ADAR1 knockdown, were
196 subjected to RNA-seq analyses to compare transcriptomic profiles between ADAR1-intact and
197 ADAR1-deficient cells (**Figure 4A, Table S1**).

198 Pathway analyses were performed to provide a glimpse of cellular functions impacted by
199 ADAR1 knockdown. The genes altered in at least three cell lines were from a variety of
200 pathways, including metabolic regulations in cancer cells and lipid and fatty acid metabolism
201 (**Figure 4B-E, Figure S4A-B, Table S2-4**). Gene set enrichment analysis (GSEA) with RNA-
202 sequencing data from MDA-MB-231 cells showed that the reduction in ADAR1 resulted in
203 significant changes in transcriptomes involved in fatty acid metabolism, but not in the ROS
204 (reactive oxygen species) pathway, iron uptake, or direct ferroptosis regulation (**Figure 4F-G,**
205 **Figure S4C-D**). GSEA results also suggest a lack of clear effect on interferon signaling or cell
206 cycle regulation (**Figure S4E-F**). Interestingly, when other metabolic pathways were evaluated,
207 ADAR1 knockdown had no effect on the glycolysis gene set but significantly altered the

208 transcriptome involved in amino acid metabolism, suggesting that ADAR1 might affect the
209 metabolic state of cancer cells beyond lipid programming (**Figure S4G-H**).

210 To narrow down the targets for further investigation, more stringent cutoff points (FDR<0.01,
211 Log2FC>0.5 or <-0.5) were applied to identify the individual genes that were most easily altered.
212 Seventeen genes (besides *ADAR*) were downregulated in at least 3 TNBC cell lines after ADAR1
213 knockdown, while only one (*MDM2*) was upregulated (**Figure 4H-I**). The induction of MDM2
214 protein in ADAR1-deficient cells was confirmed in multiple TNBC cell line models used in this
215 study, including PDX-derived WHIM12 cells (**Figure 4J and S4I).**

216 The transcription of *MDM2* is known to be regulated by ADAR1-mediated editing in 3'UTR[23,24].
217 In ADAR1-deficient MDA-MB-231 and MDA-MB-468 cells, reduced levels of A-to-I/G editing
218 were observed at the first reported editing site using both Sanger sequencing and RNA editing
219 site-specific quantitative PCR (RESS-qPCR) (**Figure 5A-D**). Multiple studies have suggested
220 that ADAR1-mediated RNA editing in *MDM2* 3'UTR can occur within a cluster of nearby
221 editing sites, potentially representing a delicate machinery for MDM2 regulation[23,25,26]. By
222 analyzing Sanger sequencing results from ADAR1-intact and -deficient MDA-MB-231 and
223 MDA-MB-468 cells, it was revealed that despite both showing induced MDM2 expression after
224 ADAR1 knockdown, the two cell lines displayed similar yet nonidentical editing profiles that are
225 sensitive to ADAR1 knockdown (**Figure S5A-B**).

226 MDM2 has been shown to promote ferroptosis sensitivity by mediating lipid remodeling,
227 including induction of PUFA levels[27]. To determine whether MDM2 is also capable of
228 promoting ferroptosis sensitivity in TNBC cells, MDA-MB-231 cells overexpressing MDM2
229 were subjected to treatment with RSL3 (**Figure 5E**). Overexpression of MDM2 sensitized

230 MDA-MB-231 cells to RSL3, albeit to a lesser extent compared to ADAR1 knockdown (**Figure**
231 **5F**). In particular, MDM2 overexpression resulted in induced sensitivity to RSL3 without
232 affecting the proliferation potential of MDA-MB-231 cells, suggesting that MDM2 plays a
233 ferroptosis-predisposing role in TNBC cells (**Figure S5C**).

234 To determine whether MDM2 promotes PUFA enrichment in TNBC cells similarly to ADAR1
235 knockdown, MDA-MB-231 cells possessing Tet-inducible MDM2 were subjected to lipidomic
236 analysis to identify PC PUFA profiles 48 and 96 hours after doxycycline treatment (**Figure**
237 **S5D**). At 48 hours, some PC PUFAs (i.e. PC34:3) were enriched. After 96 hours, a wider
238 enrichment profile emerged, including inductions of several highly unsaturated PC species, such
239 as PC42:7 and PC42:8 (**Figure 5G-I**). To confirm whether elevated ferroptosis sensitivity after
240 ADAR1 reduction can be attributed to MDM2 induction, a rescue experiment was conducted
241 with MDA-MB-231 cells treated with RSL3. The inflection point concentration of RSL3
242 (100nM) that distinguishes between ADAR1-intact and -deficient cells was used in combination
243 with MDM2 inhibitors. All three MDM2 inhibitors used (MX69, MEL23, SP141) partially
244 rescued ADAR1-deficient cells treated with RSL3 (**Figure 5J**). MDM2 was previously shown to
245 promote ferroptosis sensitivity by suppressing the activity of peroxisome proliferator-activated
246 receptor alpha (PPAR-α)[27]. Consistent with the report, an agonist of PPAR-α, pirinixic acid, was
247 shown to confer a mild but significant rescue effect. These results indicate that ADAR1 regulates
248 lipid profiles through MDM2 to protect TNBC cells from ferroptosis induction.

249 These results pointed to a paradoxical, tumor-suppressive role in TNBC for MDM2, commonly
250 known as a proto-oncogene[28]. In fact, BC patients with the basal subtype (ESR1-/HER2-) with
251 higher levels of tumor MDM2 expression have better survival outcomes (**Figure S5E**). This
252 MDM2-associated survival advantage is amplified (HR = 0.61 VS 1.25) in patients that received

253 systematic treatments (i.e. chemotherapy), potentially reflecting the fact that many existing
254 therapies, such as platinum-based agents, induce ferroptosis[29,30] (**Figure S5F-G**). One hypothesis
255 is that instead of exerting its pro-tumorigenic activity through inhibiting wild-type p53, MDM2
256 engages in more p53-independnet functions such as lipid-remodeling/ferroptosis in TNBC cells
257 that disproportionally possess deactivating p53 mutations that abrogate MDM2 interactions[31].
258 Supporting this hypothesis, high expression of MDM2 correlate strongly with better survival
259 (HR = 0.39) in patients of the basal subtype with confirmed p53 mutations (**Figure S5H**).

260 **ADAR1 reduction synergizes with cobimetinib to suppress tumorigenesis**

261 The most widely used ferroptosis inducers in preclinical studies, such as RSL3, remain distant
262 from clinical applications due to poor pharmacological profiles and excessive toxicity[32].
263 Meanwhile, many drugs currently used in clinics or tested in clinical trials have ferroptosis-
264 inducing activities[29]. Therefore, there is an opportunity to harness the lipid-remodeling effect of
265 ADAR1 inhibition to enhance the efficacy of treatments readily available to patients.

266 To identify drug candidates that synergize with ADAR1 reduction, a high-throughput screen was
267 performed to assess the effect of ADAR1 status on the sensitivity of MDA-MB-231 cells to
268 drugs included in a ferroptosis-focused library (**Figure 6A**). Drugs that synergize with ADAR1
269 reduction (shADAR1-sensitized) were expected to suppress ADAR1-deficient cells more
270 effectively, similarly to RSL3, which was used as a positive control (**Figure 6B-C**).

271 Several hits were identified to react at least twice as strongly with ADAR1-deficient cells,
272 compared to ADAR1-intact cells (**Figure 6D**). Siramesine is a lysosome disrupting agent that
273 induces ferroptosis by promoting ROS-mediated oxidative stress and reducing the expression of
274 ferroportin-1, an iron transport protein[33,34]. SB590885 is a B-Raf inhibitor that induces the

275 accumulation of ROS[35]. UC2288 is a derivative of Sorafenib, known to promote ferroptosis by
276 regulating p21 activity[36]. Alpha-Mangostin is a dietary xanthone that induces ROS activity and
277 suppresses lipogenesis[37]. Nordihydroguaiaretic acid (NDGA) is an inhibitor of 5-lipoxygenase
278 (5-LOX) that promotes PUFA peroxidation[38]. GW284543 and cobimetinib are MEK inhibitors,
279 and MEK inhibition has been shown to induce ferroptosis in multiple cancers[39,40].

280 Among the identified hits, cobimetinib is the only FDA-approved drug. Cobimetinib is approved
281 for the treatment of metastatic melanoma and histiocytic neoplasms but was also shown to
282 improve the survival of TNBC patients when combined with chemotherapy and
283 immunotherapy[41-43]. Publicly available drug response data show that cobimetinib exhibits
284 stronger activity towards TNBC compared to non-TNBC cell lines, similar to carboplatin, which
285 is known to improve the outcome of TNBC[44] (**Figure S6A-B**).

286 The orthotopic implantation mouse model described earlier was used to test the synergistic effect
287 between ADAR1 reduction and cobimetinib *in vivo* (**Figure S6C**). Upon the formation of
288 palpable tumors from MDA-MB-231 cells, mice were fed a control diet or a diet containing
289 doxycycline to induce ADAR1 knockdown before being subjected to cobimetinib treatment (oral
290 gavage at 20mg/kg weight; twice a week) for 5 weeks. The combination of the doxycycline diet
291 and cobimetinib showed superior tumor suppressive efficacy and a stronger ferroptosis
292 phenotype without observed toxicity, indicating a strong synergy between ADAR1 reduction and
293 cobimetinib to suppress tumor progression (**Figure 6E-G, Figure S6D-G**).

294 **Discussion**

295 Justified by the data shown in this study, we expanded our knowledge of ADAR1-associated
296 vulnerabilities in TNBC by showing that ADAR1 depletion sensitizes TNBC cells to ferroptosis

297 induction. Two recent studies showed that ADAR1 loss leads to overt ferroptosis phenotypes[45,46].
298 Different experimental conditions are known to affect ferroptosis phenotypes[47]. In particular,
299 CRISPR (clustered regularly interspaced short palindromic repeats)-mediated gene editing used
300 to knock out ADAR1 in these studies has been shown to alter the p53 signaling pathway, which
301 can promote ferroptosis[48,49]. Despite the disparate observations, our results agree with the
302 premise that ADAR1 plays a protective role against ferroptosis.

303 ADAR1-mediated desensitization to ferroptosis was attributed to lipid remodeling, as the
304 reduction of ADAR1 led to an increased abundance of long and highly unsaturated PUFA,
305 known to be the main drivers of ferroptosis[50]. Transcriptomic analysis revealed that MDM2 is
306 one of the commonly regulated genes in ADAR1-deficient TNBC cell lines that are sensitized to
307 ferroptosis. Consistent with its reported function in promoting ferroptosis through lipid
308 reprogramming, MDM2 was shown to be related to ADAR1-regulated ferroptosis sensitivity[27].
309 These results reveal a novel mechanism by which ADAR1 protects TNBC cells from stresses
310 that could lead to ferroptosis (**Figure 6H**). Publicly available drug response data show that the
311 sensitivity of TNBC cells to the three ferroptosis inducers used in this study (RSL3, ML162,
312 cobimetinib) is inversely correlated with their dependence on ADAR1 (**Figure S6H-J**). This
313 suggests that the dependence of TNBC cells on ADAR1 could be partially attributed to its
314 ferroptosis-protecting activity, since ferroptosis-tolerant cell lines rely on ADAR1's protection
315 against ferroptosis induction.

316 Synthetic lethality, defined as cancer cells acquiring a therapeutically targetable dependency on
317 one gene or pathway for survival following the loss or inhibition of another gene or pathway, has
318 been applied to genetically regulated metabolic vulnerabilities in TNBC[51]. Although recent
319 studies have questioned the status of ADAR1 as a *bona fide* oncogene, it is a promising target for

320 synthetic lethality applications with its ability to suppress multiple stresses directly and
321 indirectly[52]. Our model where ADAR1 inhibition primes TNBC cells for ferroptosis inducers
322 through lipid remodeling presents a novel therapeutic strategy based on recently discovered
323 TNBC biology and ferroptosis-related pharmacology. MUFA has been shown to promote cell
324 proliferation and obesity-driven metastasis of TNBC[53]. Moreover, multiple studies revealed that
325 in TNBC, MUFAs generated intracellularly and by their originating environment protect cancer
326 cells from ferroptosis[54-56]. However, PUFA abundance is positively correlated with ferroptosis
327 sensitivity in TNBC cell lines, and the increase in the PUFA/MUFA ratio has been shown to be
328 effective in sensitizing TNBC to ferroptosis[9,10,57]. A recent study identified an elevated
329 MUFA/PUFA ratio in 3D versus 2D cancer cell cultures, including TNBC, as a major obstacle to
330 translating ferroptosis inducers into preclinical/clinical settings[58]. Our *in vitro* and *in vivo* results
331 shown in this study suggest that ADAR1 inhibition is a promising way to mitigate this challenge.

332 Preliminary results showed that non-TNBC cells with ADAR1 knockdown are not sensitized to
333 RSL3. Multiple mechanisms contribute to ferroptosis resistance in non-TNBC cells, suggesting
334 higher thresholds for sensitization[59-61]. We posit that the prevalence of p53 mutations in TNBC
335 contributes to this discrepancy, as the ability of MDM2 to promote lipid remodeling and
336 ferroptosis sensitivity could be dictated by its dynamic relationship with p53. The recent
337 discovery that mutant p53 protects TNBC from ferroptosis indicates that MDM2 plays an
338 antagonistic role in promoting ferroptosis sensitivity[62]. With its many p53-independent functions,
339 both pro- and anti-tumorigenic, the complex role of MDM2 in the ADAR1 targeting strategy
340 against TNBC warrants further investigation[63].

341 Exciting opportunities are highlighted by the synergistic effect between ADAR1 reduction and
342 ferroptosis induction. In addition to the lack of clinically proven ADAR1 and ferroptosis

343 modulators, both ADAR1 inactivation and ferroptosis have been associated with pathological
344 consequences[32,64,65]. In addition to developing effective ADAR1 inhibitors, functional drug
345 repurposing offers a derisking strategy[66]. A ferroptosis-focused screen identified cobimetinib, an
346 FDA-approved MEK inhibitor with ferroptosis-inducing activity, to be sensitized with ADAR1
347 reduction. Cobimetinib and other MEK inhibitors have been shown in preclinical and clinical
348 settings to inhibit TNBC tumorigenesis[43,67]. Cobimetinib has also been shown to induce a type I
349 interferon response, indicating the potential of repurposing drugs that affect multiple pathways
350 downstream of ADAR1[68]. Future studies could examine whether other existing TNBC treatments
351 also synergize with ADAR1 inhibition with their ferroptosis-promoting activity.

352 Recent advances in ADAR1- and TNBC-related research, combined with the results shown in
353 our study, raise further questions about the implication of ADAR1's ability to regulate lipid
354 metabolism and ferroptosis sensitivity. Does ADAR1 expression or its editing profile have a
355 prognostic value to predict the response of TNBC patients to ferroptosis inducers? As both
356 ferroptosis and ADAR1 inhibition can sensitize 'immune cold' tumors to immunotherapy, can a
357 sequential or combined approach targeting ADAR1, ferroptosis, and immune checkpoints
358 minimize resistance to treatment[17,69]? Does ADAR1 protect TNBC from other metabolic
359 stresses, such as amino acid dysregulation? And how do ADAR1-regulated metabolic
360 adaptations fit into dietary interventions to improve cancer treatment[70]? ADAR1 can alter most
361 RNA species and has enormous potential for exploitation to develop innovative therapies against
362 challenging cancers such as TNBC.

363

364

365 # Methods

366 **Cell culture**

367 Breast cancer cell lines (MDA-MB-231, MDA-MB-436, MDA-MB-468, HCC1806, BT549,
368 BT20, MCF7, T47D, ZR751, SKBR3, BT474, MDA-MB-361) and human embryonic kidney
369 293T (HEK293T) cells were obtained from American Tissue Cells Consortium (ATCC,
370 Manassas, VA USA). WHIM12 cell line, as part of the patient-derived xenograft (PDX)
371 collection referred to as "Washington University Human in Mouse" (WHIM) lines, was obtained
372 from the Human and Mouse Linked Evaluation of Tumors (HAMLET) core at Washington
373 University in St. Louis. All cell lines were maintained in Dulbecco's Modification of Eagle's
374 Medium (DMEM, GE Life Sciences, Pittsburgh, PA USA) supplemented with 10% fetal bovine
375 serum (FBS, Gibco, 10091-148), Sodium Pyruvate (Cellgro, Waltham, MA USA, 30-002-CI),
376 Non-Essential Amino Acids (NEA, Cellgro, 25-030-CI), and L-glutamine (Cellgro, 25-005-CI).
377 Sensitivity of cells to ferroptosis inducing agents were tested in defined medium with low serum
378 using DMEM supplemented with 2% FBS and L-glutamine. LipoFexin (Lamda Biotech, St.
379 Louis, MO USA, TS310) was used to generate lentivirus. Fugene 6 transfection reagent
380 (Promega, E2692) was used for other transfection experiments.

381 **Plasmids**

382 Tetracycline-inducible shADAR1 was generated by cloning shADAR1 oligonucleotides (targets
383 3'UTR: GCCCACTGTTATCTTCACTTT) into Tet-pLKO.1-puro construct (Addgene #21915)
384 with AgeI and EcoRI restriction enzyme sites. Tet-inducible MDM2-overexpressing construct
385 was generated by subcloning MDM2 open-reading frame (ORF) from pCMV-myc3-MDM2
386 (Addgene #20935) into pSBtet-GP sleeping beauty vector (Addgene #60495) using the SfiI
387 restriction enzyme site. pSBtet-GP-MDM2 and pCMV(CAT)T7-SB100 transposase construct

388 (Addgene #34879) were co-transfected into MDA-MB-231 cells to generate a puromycin-
389 resistant stable cell line. Constructs containing shADAR1 (pLKO.1-shADAR1) and shNT
390 (pLKO.1-shNT; CCTAAGGTTAAGTCGCCCTCG) were obtained from MilliporeSigma
391 (MISSION® Lentiviral shRNA; TRCN0000050788) and Addgene (#136035), respectively.

392 **Lentiviral production and transduction**

393 To generate lentivirus, HEK293T cells were transfected using LipoFexin with pCMV-VSV-G
394 (Addgene #8454), pCMV-ΔR8.2 (Addgene #8455), and expression constructs. Growth medium
395 was replaced with fresh medium 24hr after transfection, and supernatants containing lentivirus
396 were harvested 24hr later. For transduction, one million cells were infected with lentivirus for
397 24hr in the presence of 10 μg/ml protamine sulfate to facilitate viral entry. Transduced cells were
398 selected with puromycin (2 μg/ml) (Gibco, A11138-03).

399 **Cell viability assay**

400 For cell viability assays, cells were plated at a density of 1,000 to 3,000 cells per well on a 96-
401 well plate and left to grow overnight in complete growth medium at 37°C. Cells were then
402 treated with the indicated drugs in equal volume at 2× desired concentration and left to incubate
403 for 72 h. Cells were then incubated with CellTiter-Glo® 2.0 Reagent (Promega, Madison, WI,
404 USA, G924C) for 1h at room temperature, and viability was read out according to the
405 manufacturer's protocol on a GloMax Navigator Microplate Luminometer (Promega, GM2000).
406 The half-maximal inhibitory concentration (IC_{50}) was determined using a nonlinear regression
407 model using Prism 10 software (GraphPad, https://www.graphpad.com).

408 Chemicals used during viability assays in this study include RSL3 (Selleck chemicals, #S8155),
409 ML162 (Selleck chemicals, #S4452), UAMC-3203 (MedChemExpress, #HY-112909),

410 Ferrostatin-1 (Selleck chemicals, #S7243), Liproxstatin-1 (Selleck chemicals, #S7699), SP-141
411 (MedChemExpress, #HY-110182), MEL23 (MilliporeSigma, #373227), MX69 (Selleck
412 chemicals, #S8403), and pirinixic acid (MedChemExpress, #HY-16995).

413 **Lipid peroxidation assay; Glutathione activity assay; Ferrous iron assay**

414 Biochemical assays were performed to evaluate ferroptosis phenotypes or molecular mechanisms
415 contributing to cells' sensitivity to ferroptosis induction. Level of lipid peroxidation was
416 determined by **1)** measuring its natural byproduct malondialdehyde (MDA) using MDA
417 Colorimetric/Fluorometric Assay (Abcam, Cambridge, UK, ab118970), or by **2)** staining and
418 comparing levels of reduced and oxidized forms of lipid peroxidation probe BODIPY^{TM} 581/591
419 C11 (Image-iT^{TM} Lipid Peroxidation Kit, Thermo Fisher Scientific, #C10445), according to
420 manufacturer's instruction. Intracellular oxidative stress level was determined by measuring the
421 ratio between reduced (GSH) and oxidized (GSSG) forms of Glutathione using GSH/GSSG
422 Ratio Detection Assay (Abcam, ab205811) according to manufacturer's instruction. Ferrous iron,
423 which drives ferroptosis, was measured by FerroOrange staining (Dojindo, Japan, F374)
424 according to the manufacturer's instructions. Quantification of signal intensity was performed
425 using ImageJ software (NIH, Bethesda, MD USA).

426 **Untargeted lipidomic analysis with reversed-phase liquid chromatography (RPLC)**

427 Cells were washed with cold PBS 3 times, cold molecular biology grade water (Corning,
428 Glendale, AZ, 46-000-CM) 3 times, metabolically quenched with cold methanol for 5 min,
429 scraped harvested, and centrifuged at 10,000 × g for 5 min to remove supernatant. Cell pellets
430 were dried using CentriVap Concentrator (Labconco, Kansas City, MO, 79700-00) and stored in
431 -80°C before extraction of metabolites. Cold extraction buffer containing
432 Methanol:Acetonitrile:Water at 2:2:1 ratio was added to the pellets. Samples were then subjected

433 to 3 times of 30-sec vortex → 1-min liquid nitrogen bath → 10-sec thaw → 10-min bath
434 sonication at 25°C (Fischer Scientific, CPXH Series Model 3800 Heated Ultrasonic Cleaner),
435 before being stored at -20°C for 2 hours to overnight. After centrifuging at 14000 RPM at 4°C
436 for 10 min, sample supernatants were transferred to new Eppendorf tubes and speed dried for 2
437 hours. BCA Protein Assay was performed on cell pellets in advance to determine protein
438 concentration. Isopropanol:Methanol at 1:1 ratio was added at 1µL per 2.5µg of proteins to the
439 residue and subjected to 2 times of 5-min bath sonication at 25°C → 1-min vortex, before being
440 stored at 4°C for 1 hour to overnight. After centrifuging at 14000 RPM at 4°C for 10 min,
441 supernatants were transferred to LC vials for LC/MS analysis. Following extraction, an internal
442 standard (Avanti Research, SPLASH® LIPIDOMIX® Mass Spec Standard, 330707) was spiked
443 into each experimental sample for quality control.

444 An aliquot (4µL) of the extracted sample was injected onto a Waters HSS T3 1.8µM,
445 2.1x150mm column with a 1.8µM, 2.1x50mm guard column connected to 1290 Infinity II LC.
446 The columns were used with the following buffers and gradients: Mobile Phase A = 40% water,
447 60% Acetonitrile, 0.1% Formic Acid, 10mM Ammonium Formate, 2.5µM Medronic Acid;
448 Mobile Phase B = 90% Isopropanol, 10% Acetonitrile, 0.1% Formic Acid, 10mM Ammonium
449 Formate; Needle Wash = 70% Mobile Phase A solution + 30% Mobile Phase B solution; Seal
450 Wash = 9:1 Water:Isopropanol. All solutions were mixed and degassed for 10 min before use.
451 The binary pump was operated at 70% A + 30% B from 0 - 17 min, 25% A + 75% B 0% B from
452 17 - 20 min, 15% A + 85% B from 20 - 23 min, 100% B from 23 - 27 min, and 70% A + 30% B
453 thereafter at constant 0.25 mL/min flow rate. MS detection was carried out using Agilent 6545
454 Q-TOF with 150-1,200 Da mass range. Lipid Annotator (Version 1.0, Agilent) was used to

455 generate a target list for all lipids detected. LC/MS results were analyzed and visualized with
456 MetaboAnalyst (McGill University, https://www.metaboanalyst.ca).

457 **Bulk RNA sequencing and analysis**

458 Total RNA was isolated from cells transduced with shNT or shADAR1 lentivirus for 24hr,
459 followed by 24hr of puromycin selection, using miRNeasy Mini Kit (Qiagen, Hilden, Germany,
460 217004) including on-column DNase digestion following the manufacturer's protocol. Samples
461 were prepared according to RiboErase library kit (Roche) manufacturer's protocol, indexed,
462 pooled, and sequenced on an Illumina NovaSeq S4. Base calls and demultiplexing were
463 performed with Illumina's bcl2fastq software and a custom python demultiplexing program with
464 a maximum of one mismatch in the indexing read. RNA-seq reads were then aligned to the
465 Ensembl release 76 primary assembly with STAR version 2.5.1a1. Gene counts were derived
466 from the number of uniquely aligned unambiguous reads by Subread:featureCount version 1.4.6-
467 p52. Sequencing performance was assessed for the total number of aligned reads, total number of
468 uniquely aligned reads, and features detected. All gene counts were then imported into the
469 R/Bioconductor package EdgeR and TMM normalization size factors were calculated to adjust
470 for samples for differences in library size. Ribosomal genes and genes not expressed in the
471 smallest group size minus one sample greater than one count-per-million were excluded from
472 further analysis. The TMM size factors and the matrix of counts were then imported into the
473 R/Bioconductor package Limma. Weighted likelihoods based on the observed mean-variance
474 relationship of every gene and sample were then calculated for all samples with
475 voomWithQualityWeights. The performance of all genes was assessed with plots of the residual
476 standard deviation of every gene to their average log-count with a robustly fitted trend line of the
477 residuals. Differential expression analysis was performed to analyze differences between

478 conditions and raw p-values and Benjamini-Hochberg false-discovery rate (FDR) adjusted p-
479 values were determined to filter results based on cut-off. Biological and functional pathways
480 analyses, as well as gene set enrichment analyses were performed with the Enrichr platform
481 (Icahn School of Medicine at Mount Sinai, https://amp.pharm.mssm.edu/Enrichr), the
482 GeneOntology enrichment tools (Gene Ontology Consortium, https://geneontology.org/docs/go-
483 consortium), and the Gene Set Enrichment Analysis (GSEA) software (Broad Institute/UC San
484 Diego, https://www.gsea-msigdb.org/gsea). $p<0.05$ was used as the cutoff to identify genes
485 commonly regulated among 4 TNBC cell lines, and FDR<0.1 was used as the cutoff to identify
486 regulated genes in MDA-MB-231 cells for GSEA analysis. Relevant molecular signatures
487 databases (MSigDB) were selected for GSEA analysis. When multiple MSigDB files exist for a
488 similar pathway, the one with the biggest gene list was preferred. MSigDB used in this study
489 include WP_FERROPTOSIS, REACTOME_FATTY_ACID_METABOLISM,
490 HALLMARK_REACTIVE_OXYGEN_SPECIES_PATHWAY,
491 REACTOME_IRON_UPTAKE_AND_TRANSPORT, REACTOME_CELL_CYCLE,
492 REACTOME_INTERFERON_SIGNALING, HALLMARK_GLYCOLYSIS, and
493 GOBP_AMINO_ACID_METABOLIC_PROCESS.

494 **Immunoblotting (western blotting) analysis**

495 Cells were washed with phosphate-buffered saline (PBS, Corning, #21-031-CM), scrape
496 harvested, centrifuged at 1000 × g for 5 min, and lysed with RIPA buffer (20mM Tris-HCl
497 pH7.5, 150mM NaCl, 1mM EDTA, 1% NP-40, 0.1% SDS, 0.1% Deoxycholate) supplemented
498 with 10mM PMSF and HALT protease inhibitor cocktail (Thermo Fisher Scientific, #78440).
499 Lysates were clarified by centrifugation, and the protein concentration was determined using DC
500 protein assay system (Bio-Rad, Hercules, CA USA, #5000113). Equal amount of protein was

501 resolved by sodium dodecyl sulfate-polyacrylamide gel electrophoresis (SDS-PAGE) using
502 Criterion TGX Stain-Free Precast Gels (Bio-Rad, #5678094) and transferred onto Immobilon-P
503 membranes (MilliporeSigma, ISEQ85R). Primary antibodies used in this study include anti-
504 ADAR1 antibody (Santa Cruz Biotechnology, sc-73408; RRID:AB_2222767; 1:300), anti-
505 GAPDH antibody (Bethyl Laboratories, A300-641A; RRID:AB_513619; 1:10,000), anti-MDM2
506 antibody (Cell Signaling Technology, #86934; RRID:AB_2784534; 1:1,000), and anti-Myc-tag
507 antibody (Cell Signaling Technology, #2278; RRID:AB_490778; 1:1,000). Secondary antibodies
508 conjugated to Horseradish peroxidase were used at a dilution of 1:5-10,000 (Jackson
509 Immunochemicals, West Grove, PA USA). Clarity Western ECL Substrate (Bio-Rad, #170-
510 5061) was then applied to blots and protein levels were detected using autoradiography with
511 ChemiDoc XRS+ Imager (Bio-Rad).

512 **RNA editing site-specific quantitative PCR (RESS-qPCR)**

513 Total RNA was isolated from lentivirus-transduced cells using RNeasy Plus Mini Kit including
514 on-column DNase digestion following the manufacturer's protocol. To eliminate any residual
515 genomic DNA contamination, TURBO DNA-free^{TM} Kit (ThermoFisher Scientific, AM1907)
516 was used to further clean up isolated RNAs. RNAs free of genomic DNA were reverse
517 transcribed to cDNAs using the High-Capacity cDNA Reverse Transcription Kit (ThermoFisher
518 Scientific, #4368814). Primers were designed to amplify MDM2-WT (Forward:
519 ATAGGACTGAGGTAATTCTGCACAGCA; Reverse:
520 ATAATGCTTGGAGGACCTCCACATGT) and MDM2-Edited (Forward:
521 TAAATGGCCAAAGGGATTAGTAGTGTG; Reverse:
522 AAGAGATTCTGCTTGGTTGTAGCTGAAG). Quantitative PCR was performed using iTaq
523 Universal SYBR Green Supermix (Bio-Rad, #1725125) on the CFX96 Touch Real-Time PCR

524 Detection System (Bio-Rad, #1845097). The relative RNA editing level (Edit/Wild-Type RNA
525 ratio) was calculated as $2^{-(Ct\ Edit - Ct\ WT)}$.

526 **Sanger sequencing to detect RNA editing**

527 Isolated RNAs free of genomic DNA were used for Sanger sequencing analysis to verify RNA
528 editing events. PCR was performed using the high-fidelity Phusion PCR kit according to the
529 manufacturer's instructions (New England Biolabs, Ipswich, MA, E0553). "Outer" primers were
530 used to produce amplicons flanking the editing site about 50-150 bp on either side to ensure
531 successful sequencing analysis: MDM2 3'UTR Motif 1 (Forward:
532 GCCTAGCAATGATCTAGAAGCAG; Reverse: GCACACCCATCAGCTCAAATAT), MDM2
533 3'UTR Motif 2 (Forward: ATAGGACTGAGGTAATTCTGCACAGCA; Reverse:
534 AAGAGATTCTGCTTGGTTGTAGCTGAAG). Successful PCRs were verified by DNA gel
535 electrophoresis and amplicons were extracted from the gel using Monarch gel extraction kit
536 (BioRad, T1020S) according to manufacturer's instructions and submitted for sequencing
537 analysis (IDT Technologies). Sanger sequencing was performed using the outer primers (A/G
538 were read for WT/Edited if forward primers were used; T/C were read if reverse primers were
539 used) used for PCR, and sequence chromatograms were analyzed and converted to A/G reading
540 for presentation purposes using Chromas software (Technelysium,
541 https://technelysium.com.au/wp/chromas).

542 **Drug screening with ferroptosis-focused library**

543 MDA-MB-231 cells treated with shNT (ADAR1-intact) or shADAR1 (ADAR1-deficient) were
544 screened against the ferroptosis-focused drug library (MedChemExpress, HY-L051) at the High
545 Throughput Screening Center (HTSC) at Washington University in St. Louis. CellTiter-Glo®

546 Viability Assay was utilized to determine cell viability upon drug treatment. Cells were prepared
547 in defined medium with low serum using DMEM supplemented with 2% FBS and L-glutamine.
548 All drugs in the library were pre-dispensed into 96-well sterile polypropylene plates (Corning,
549 Axyen) using a Hummingbird and subsequently diluted with media to produce intermediate
550 plates at 20µM and 2µM. Diluted compounds were then transferred using a BiomekFX
551 (Beckman Coulter) to 96-well white cell culture plates (Greiner Bio-One, Monroe, NC, 655083)
552 (50µl/well, 18 plates total with 9 plates for each experimental group. Select wells containing
553 DMSO alone served as controls. Cells were seeded (15,000 cells in 50µl cell culture media per
554 well) using the Multidrop 384 dispenser (Thermo Fisher Scientific, 24291). Plates were kept at
555 room temperature for 30 min before being moved to the incubator (37°C, 5% CO_2) for 24h. On
556 day 2, viability Assays were performed using the integrated and automated platform (Beckman
557 Coulter), with library plate-matched ADAR1-intact and ADAR1-deficient samples alternating
558 between screening steps: Cell plates were equilibrated at room temperature for 30 min in a
559 Cytomat MPH incubator. CellTiter-Glo® reagent (100µl/well) was added with a Multidrop 384
560 dispenser. Plates were shaken at 250 rpm for 2 min with a Teleshake followed by room
561 temperature incubation for 1h in a Cytomat MPH incubator. Luminescence was measured (1
562 sec/well after a 1 min delay) with a Perkin Elmer Envision plate reader. To monitor assay
563 performance, Coefficient of variations (CVs) and Z'-factors for DMSO-treated and no-cell
564 control samples were determined. All screening plates were confirmed to display high quality
565 assay metrics (CVs < 10%; Z'-factors > 0.8). All test wells were normalized to no-treatment
566 samples on the same plate. Relative cell viability was compared between ADAR1-intact and
567 ADAR1-deficient samples, and the cut-off was set at 51% to discriminate hits from no-hits. Drug

568 screening results were analyzed and visualized with CDD vault (Collaborative Drug Discovery,
569 https://www.collaborativedrug.com).

570 **Mammary fat pad orthotopic implantation**

571 Immuno-deficient NOD scid gamma (NSG) female mice at 6-8 weeks old were purchased from
572 Jackson Laboratory (Bar Harbor, ME, USA, #005557) and placed on Teklad Global 18% protein
573 rodent diet (Envigo, Indianapolis, USA, T.2918.15) 3 days before implantation. 1.5 x 10^5 MDA-
574 MB-231 cells were harvested and resuspended in PBS, mixed with Matrigel® Matrix Basement
575 Membrane (Corning, Waltham, USA, #354230) at 1:1 volume ratio, and kept at 4°C until
576 implantation. In total 100µl of cells-Matrigel solutions were injected into the right inguinal
577 mammary glands of NSG mice. Ten days after the implantation, palpable tumors were detected
578 and half of the mice were switched to doxycycline-containing diet (Envigo, 625mg/kg,
579 TD.01306). RSL3 (100mg/kg weight; IP injection) and cobimetinib (MedChemExpress, HY-
580 13064; 20mg/kg weight; Oral gavage) were freshly prepared in DMSO:Corn oil
581 (MedChemExpress, HY-Y1888) before treatment, starting 3 days after the diet switch. Tumors
582 were measured using a caliper once per week, and tumor volumes were calculated using the
583 following formula: $L \times W^2 \times 0.52$ (L and W represent the large and small diameter of the tumor,
584 respectively). Mice were euthanized 6 weeks post implantation or before tumors reached 2 cubic
585 cm in size. Tumors were dissected from the mice for weight measurement and subsequently
586 fixed in 10% formalin, before transferred to 70% ethanol for processing to prepare formalin-
587 fixed paraffin-embedded (FFPE) tissue blocks. All animal-related experimental procedures were
588 performed in compliance with the guidelines given by the American Association for
589 Accreditation for Laboratory Animal Care and the U.S. Public Health Service Policy on Human
590 Care and Use of Laboratory Animals. All animal studies were approved by the Washington

591 University Institutional Animal Care and Use Committee (IACUC) in accordance with the
592 Animal Welfare Act and NIH guidelines (Protocol 20220144).

593 **Immunohistochemistry (IHC)**

594 Tumor FFPE tissue blocks were sectioned at 5μm thickness. Hematoxylin and eosin (H&E)
595 staining was performed for histological evaluations. For immunohistochemistry, sections were
596 stained using a Bond RXm autostainer (Leica, Buffalo Grove, IL USA). Primary antibodies for
597 ADAR1-p150 (Abcam, ab126745; RRID:AB_11145661) and 4-Hydroxynonenal (4HNE,
598 ThermoFisher Scientific, MA5-27570; RRID:AB_2735095) were diluted 1:100 in Antibody
599 Diluent (Leica, AR9352). Briefly, slides were baked at 65°C for 15min and automated software
600 performed dewaxing, rehydration, antigen retrieval, blocking, primary antibody incubation, post
601 primary antibody incubation, detection (DAB chromogen; 3,3′-diaminobenzidine), and
602 hematoxylin counterstaining using Bond reagents (Leica, DS9800 system). Samples were then
603 removed from the machine, dehydrated through ethanol and xylenes, mounted and cover slipped
604 before being imaged using Zeiss Axioskop 2 MOT microscope. Quantification of DAB signals
605 was performed using ImageJ Fiji package.

606 **Bioinformatic analysis and data availability**

607 Bioinformatic analyses to assess relationships among gene expression, drug response, gene
608 dependency and metabolomics in breast cancer cell lines were performed using the DepMap
609 public data (depmap.org) with the TNBC (HCC1187, HS578T, HCC1599, DU4475, BT549,
610 HCC1143, BT20, MDA-MB-436, HCC1806, HCC70, HCC2157, HCC1395, MDA-MB-231,
611 MDA-MB-468, MDA-MB-453) and non-TNBC (SKBR3, MCF7, KPL1, MDA-MB-134VI,
612 ZR751, EFM192A, T47D, AU565, HCC1419, EFM19, HCC1500, HCC1428, UACC893,
613 UACC812, HCC202, HCC2218, MDA-MB-175VII, BT483, ZR7530, MDA-MB-415, BT474,

614 HCC1569, MDA-MB-361) groups. The results published here are in whole or part based upon
615 data generated by Cancer Target Discovery and Development (CTD²) Network
616 (https://ccg.cancer.gov/ccg/research/functional-genomics/ctd2/data-portal) established by the
617 National Cancer Institute's Center for Cancer Genomics. Kaplan-Meier plots for breast cancer
618 patients' survival outcome were obtained from Kaplan-Meier Plotter (https://KMplot.com), using
619 the mRNA gene chip data with auto select best cutoff. The secondary RNA structure of MDM2
620 3'UTR was predicted and visualized with RNAfold web server (ViennaRNA Web Services,
621 https://rna.tbi.univie.ac.at). RNA-seq data from this study are available at the Gene Expression
622 Omnibus under accession number GSE286185.

623 **Statistical analysis**

624 All *in vitro* and *in vivo* data are reported as the mean ± SD unless stated otherwise, and statistical
625 analyses were performed using GraphPad Prism 10. The two-tailed unpaired student t test was
626 performed for experiments comparing between two experimental groups. One-way ANOVA
627 with Tukey's multiple comparisons was used for statistical analysis of all other experiments
628 unless stated otherwise. Tumor volume analyses were performed by **1)** comparing AUC (area
629 under curve) between experimental groups using one-way ANOVA, and **2)** comparing weekly
630 measured tumor volumes between groups using two-way ANOVA with Tukey's multiple
631 comparison. Pearson correlation coefficient and/or Spearman's rank correlation coefficient were
632 calculated to assess correlations between two data sets. Statistical significance was evaluated
633 using p-value, which is shown in the numerical format. Lower p-values reject the null hypothesis
634 more strongly, and p-value <0.05 is generally considered statistically significant.

635

636

637 **Resource availability**

638 **Lead contact**

639 Requests for further information and resources should be directed to and will be fulfilled by the
640 lead contact, Jason D. Weber (jweber@wustl.edu).

641 **Materials availability**

642 All unique/stable reagents generated in this study are available from the lead contact with a
643 completed materials transfer agreement.

644 **Data and code availability**

645 All data reported in this paper will be shared by the lead contact upon request. This paper does
646 not report original code. Any additional information required to reanalyze the data reported in
647 this paper is available from the lead contact upon request.

648 **Acknowledgements**

649 We thank the Division of Comparative Medicine at Washington University in St. Louis for
650 housing the mouse colony. We thank the Denardo lab for processing the fixed tumor tissues. We
651 thank the Histology and Morphometry Core, Musculoskeletal Research Center (supported by
652 NIH P30 AR074992), for sectioning the tumor samples and performing H&E staining. We thank
653 the support by the Genome Technology Access Center (GTAC) at McDonnell Genome Institute
654 (MGI) Symposium Pilot Project Funding to perform RNA-seq analyses (Catrina Fronick and
655 Michael Heinz for logistics; Toni Sinnwell, Elliott Klotz, and Eric Tycksen for quality control,
656 sequencing and analyses). We acknowledge the Just-In-Time (JIT) Core Usage Funding Program
657 to support the collaboration with HTSC for drug screening. Both GTAC@MGI Symposium Pilot
658 Project and JIT programs are funded through the Institute of Clinical and Translational Sciences

(ICTS), Washington University in St. Louis. ICTS was supported by the National Center for Advancing Translational Sciences (NCATS) grant UL1TR002345. This work was supported by R01CA262804 (JDW) from National Cancer Institute (NCI), and W81XWH-21-1-0476 and W81XWH-21-1-0466 from the Congressionally Directed Medical Research Programs (CDMRP), Department of Defense (JDW). C-P. K received support from Transdisciplinary Research in Energetics and Cancer (TREC) Training Workshop R25CA203650 from NCI and TL1 Translational Sciences Postdoctoral Program TL1TR002344 from National Center for Advancing Translational Sciences. L.S.T. is supported by R25HG006687 and T32GM148405 from National Human Genome Research Institute and National Institute of General Medical Sciences, respectively.

Author contributions

C-P. Kung: Conceptualization, investigation, methodology, formal analysis, project administration, writing–original draft, writing–review and editing. **N.D. Terzich:** investigation, methodology, formal analysis. **M.X.G. Ilagan:** investigation, methodology, formal analysis, writing–review and editing. **M.J. Prinsen:** Investigation, methodology, formal analysis. **M. Kaushal:** Investigation, methodology, formal analysis. **R.D. Kladney:** Investigation, methodology. **J.H. Weber:** Investigation. **A.R. Mabry:** Investigation. **L.S. Torres:** Investigation. **E.R. Bramel:** Investigation. **E.C. Freeman:** Investigation. **T. Sabloak:** Investigation. **K.A. Cottrell:** Investigation. **S. Ryu:** Investigation. **W.M. Weber:** Investigation. **L.B. Maggi Jr.:** investigation, writing–review and editing. **L.P. Shriver:** investigation, methodology, writing–review and editing. **G.J. Patti:** funding acquisition, investigation, writing–review and editing. **J.D. Weber:** Conceptualization, resources, supervision, funding acquisition, writing–original draft, writing–review and editing.

682 **Declaration of interests**

683 G.J. Patti is the Chief Scientific Officer of Panome Bio, a scientific advisory board member for
684 Cambridge Isotope Laboratories, and has a collaborative research agreement with Agilent
685 Technologies.

686 **Supplementary information**

687 Supplementary Figure S1-S6

688 Supplementary Table 1. Genes altered in ADAR1-deficient TNBC cell lines

689 Supplementary Table 2. Signaling pathways altered upon ADAR1 knockdown

690 Supplementary Table 3. Disease-related biological functions altered upon ADAR1 knockdown

691 Supplementary Table 4. Biological pathways altered upon ADAR1 knockdown

692

693

694

695

696

697

698

699

700

701

702

703

704

705 **Figure 1. ADAR1 protects TNBC cells from ferroptosis induction**

706 **A)** Light micrographs of ADAR1-intact (shNT) and -deficient (shADAR1) MDA-MB-231 cells
707 treated with RSL3 for 24h. Cell viability analyses were performed to determine IC_{50} values of
708 ferroptosis inducers **B)** RSL3 and **C)** ML162 for MDA-MB-231 cells. IC_{50} of RSL3 were
709 determined for **D)** MDA-MB-436, **E)** HCC1806, and **F)** MDA-MB-468 TNBC cells, as well as
710 **G)** MCF7, **H)** T47D, and **I)** BT474 non-TNBC cells. Cell viability graphs are representatives of
711 three replicates. **J)** Average levels of shADAR1-mediated sensitization to RSL3 among TNBC
712 (red bars) and non-TNBC (nTNBC; blue bars) cell lines. Dashed line denotes an arbitrarily
713 determined threshold (IC_{50}shNT/IC_{50}shADAR1 = 1.5) for notable shADAR1-mediated
714 sensitization to RSL3. **K)** IC_{50} values of RSL3 for PDX-derived TNBC cell line WHIM12. FC
715 (fold-change) represent levels of shADAR1-mediated sensitization to RSL3.

716 **Figure 2: Combining ADAR1 reduction with RSL3 suppresses orthotopically implanted**
717 **MDA-MB-231 xenograft progression *in vivo***

718 **A)** Immunoblot analysis showed similar levels of ADAR1 knockdown in doxycycline-treated
719 MDA-MB-231 cells with Tet-inducible shADAR1 compared to cells treated with shADAR1-
720 containing lentivirus. Images are representative of three replicates. GAPDH, loading control. **B)**
721 MDA-MB-231 cells (1.5 X 10^5 per mouse) with Tet-inducible shADAR1 were implanted into
722 mammary fat pads of female NSG mice. Ten days post implantation, half of the mice were
723 switched to doxycycline-containing (625mg/kg) diet, followed by RSL3 treatments (100mg/kg
724 weight; i.p. injection twice a week) for 5 weeks. **C)** Progression of overall tumor volumes, n=5-9
725 each group. Error bars mark standard deviation. **D)** Quantification of areas under curve (AUC)
726 from C). Error bars mark standard deviation. **E)** Two-way ANOVA analysis to compare weekly
727 measured overall tumor volumes. Statistically significant p-values (<0.05) were highlighted in
728 red. **F)** Representative images of IHC staining of H&E, ADAR1 (p150 isoform), and 4HNE in
729 resected tumor samples. Scale bar, 200µm. **G)** Quantification of IHC staining intensity of 4HNE.
730 Error bars mark standard deviation. N=4-6 each group.

731 **Figure 3: ADAR1 reduction leads to lipid remodeling**

732 **A)** Key regulators of ferroptosis. GSH, Glutathione. PL, phospholipid. MUFA, monounsaturated
733 fatty acid. PUFA, polyunsaturated fatty acid. PM, plasma membrane. **B)** Heatmap of lipidomic
734 analysis in MDA-MB-231 cells upon ADAR1 knockdown. PC, phosphatidylcholines. **C)**
735 Relative abundance of PC species listed in the order of carbon chain length or **D)** lipid
736 unsaturation. Values were log10 transformed, mean centered, and shown as mean over standard
737 deviation ratio. n=5. Red dots denote ADAR1-intact, and blue dots denote ADAR1-deficient
738 samples. **E)** Enrichment of PC species with different carbon chain lengths and **F)** different
739 unsaturation levels (SFA, 0 double-bond; MUFA, 1 double-bond; PUFA, ≥ 2 double-bond;
740 XPUFA, ≥ 4 double-bond) upon ADAR1 knockdown. Data from individual samples (n=4) were
741 normalized to the average intensity in shNT samples. **G)** Relative abundance of PC38:4 between
742 ADAR1-intact and -deficient MDA-MB-231 cells. Data from individual samples (n=5) were
743 divided by the overall average of PC38:4 intensity in all samples and log2 transformed.
744 Abundance of **H)** PC32:0, **I)** PC32:1, and **J)** PC34:1 positively correlate with *ADAR* (encoding

745 ADAR1) expression level in TNBC (n=13), but not non-TNBC (n=23), cell lines. Data was
746 extracted from metabolomics data set from DepMap (depmap.com).

747 **Figure 4: Transcriptomic regulation in TNBC cells upon ADAR1 knockdown**

748 **A)** RNA sequencing to identify significantly altered genes in ADAR1-deficient TNBC cells. **B)**
749 Downregulated and **C)** upregulated genes in ADAR1-deficient TNBC cell lines. **D)** Significantly
750 altered signaling pathways (BioPlanet_2019) and **E)** disease-related biological functions
751 (PheWeb_2019) in ADAR1-deficient TNBC cells. Genes altered in at least 3 cell lines are
752 included. **F)** GSEA enrichment plot of ferroptosis and **G)** fatty acid metabolism genes in
753 ADAR1-deficient MDA-MB-231 cells. **H)** The most significantly downregulated and **I)**
754 upregulated genes (FDR<0.01, Log2FC<-0.5 or >0.5) in ADAR1-deficient TNBC cells. Genes
755 altered in at least 3 cell lines are listed on the right. **I)** Immunoblot analysis showed MDM2
756 induction upon ADAR1 knockdown in MDA-MB-231 cells. Images are representative of three
757 replicates. GAPDH, loading control.

758 **Figure 5: ADAR1 regulates MDM2 expression to dictate ferroptosis sensitivity**

759 **A)** Reported ADAR1 editing motifs (red bracket) and a representative site (bolded and
760 underlined) in MDM2 3'UTR. Numbers mark the location within the open reading frame. **B)**
761 Predicted RNA secondary structure of the entire MDM2 3'UTR and the reported ADAR1 editing
762 motifs (dashed red box) and a specific site (circled in red in the zoomed-in square). **C)** Reduced
763 editing of the representative MDM2 site in ADAR1-deficient TNBC cells. A (green) and G
764 (black) reading represent non-edited and edited RNA, respectively. Ratio of G/A peak heights
765 indicates editing levels. Sequence chromatograms shown are representative of 3 replicates. **D)**
766 RESS-qPCR showed reduced editing of the MDM2 3'UTR site in ADAR1-deficient cells. n=3.
767 Error bars mark standard error. **E)** Immunoblot analysis showed MDM2 (Myc-tagged)
768 overexpression in MDA-MB-231 cells. GAPDH, loading control. **F)** IC_{50} of RSL3 for MDA-
769 MB-231 cells with MDM2 overexpression. Graph is representative of three replicates. FC, fold-
770 change of MDM2-mediated sensitization (IC_{50}Control/IC_{50}MDM2) to RSL3. **G)** Relative
771 abundance of PUFA PC species, listed in the order of lipid unsaturation, in MDA-MB-231 cells
772 with MDM2 overexpression (red dots) for 48h (left panel) and 96 h (right panel). n=5. **H)**
773 Relative abundance of PC42:7 between control (Ctrl) and MDM2-overexpressing MDA-MB-231
774 cells. n=5. **I)** Significantly enriched PUFA PC species (red dots) in MDM2-overexpressing (96h)
775 MDA-MB-231 cells. **J)** Relative cell viability within ADAR1-intact and -deficient MDA-MB-
776 231 cells treated with RSL3 (100nM), as well as ADAR1-deficient cells co-treated with MDM2
777 inhibitors MX69 (10μM), MEL23 (10μM), and SP-141 (10μM), or PPAR-α agonist pirinixic
778 acid (PA; 10μM) for 72h. n=3. Error bars mark standard error.

779 **Figure 6: ADAR1 reduction synergizes with cobimetinib to suppress tumorigenesis**

780 **A)** Drug screen to identify shADAR1-sensitized ferroptosis modulators. **B)** shADAR1-sensitized
781 hits (red dots) preferentially reduce viability of ADAR1-deficient cells. X and Y axis represent
782 cell viability for ADAR1-intact and -deficient cells, respectively. **C)** Screening result with a
783 ferroptosis-focused library (654 small molecules) in MDA-MB-231 cells. Data were normalized

784 to DMSO-treated cells. RSL3 was included as positive control. Black dashed line denotes
785 expected locations for molecules without discriminating activity. **D)** List of hits (viability ratio
786 shADAR1/shNT ≤ 0.51) identified, ranked by cell viability ratio. **E)** Progression of overall tumor
787 volumes, n=5-10 each group. Error bars mark standard deviation. **F)** Quantification of areas
788 under curve (AUC) from F). Error bars mark standard deviation. **G)** Two-way ANOVA analysis
789 to compare weekly measured overall tumor volumes. Statistically significant p-values (<0.05)
790 were highlighted in red. **H)** ADAR1 protects TNBC cells from ferroptosis through regulating
791 MDM2 and lipid compositions between MUFA and PUFA. FIN, ferroptosis inducer.

792

793

794

795

796

797

798

799

800

801

802

803

804

805

806

807

808

809

810

References

1 Obidiro, O., Battogtokh, G. & Akala, E. O. Triple Negative Breast Cancer Treatment Options and Limitations: Future Outlook. *Pharmaceutics* **15**, doi:10.3390/pharmaceutics15071796 (2023).

2 Loizides, S. & Constantinidou, A. Triple negative breast cancer: Immunogenicity, tumor microenvironment, and immunotherapy. *Front Genet* **13**, 1095839, doi:10.3389/fgene.2022.1095839 (2022).

3 Zhou, L. & Yu, C. W. Epigenetic modulations in triple-negative breast cancer: Therapeutic implications for tumor microenvironment. *Pharmacol Res* **204**, 107205, doi:10.1016/j.phrs.2024.107205 (2024).

4 Munkacsy, G., Santarpia, L. & Gyorffy, B. Therapeutic Potential of Tumor Metabolic Reprogramming in Triple-Negative Breast Cancer. *Int J Mol Sci* **24**, doi:10.3390/ijms24086945 (2023).

5 Stockwell, B. R. Ferroptosis turns 10: Emerging mechanisms, physiological functions, and therapeutic applications. *Cell* **185**, 2401-2421, doi:10.1016/j.cell.2022.06.003 (2022).

6 Verma, N. *et al.* Synthetic lethal combination targeting BET uncovered intrinsic susceptibility of TNBC to ferroptosis. *Sci Adv* **6**, doi:10.1126/sciadv.aba8968 (2020).

7 Beatty, A. *et al.* Metabolite Profiling Reveals the Glutathione Biosynthetic Pathway as a Therapeutic Target in Triple-Negative Breast Cancer. *Mol Cancer Ther* **17**, 264-275, doi:10.1158/1535-7163.MCT-17-0407 (2018).

8 Timmerman, L. A. *et al.* Glutamine sensitivity analysis identifies the xCT antiporter as a common triple-negative breast tumor therapeutic target. *Cancer Cell* **24**, 450-465, doi:10.1016/j.ccr.2013.08.020 (2013).

9 Beatty, A. *et al.* Ferroptotic cell death triggered by conjugated linolenic acids is mediated by ACSL1. *Nat Commun* **12**, 2244, doi:10.1038/s41467-021-22471-y (2021).

10 Lorito, N. *et al.* FADS1/2 control lipid metabolism and ferroptosis susceptibility in triple-negative breast cancer. *EMBO Mol Med* **16**, 1533-1559, doi:10.1038/s44321-024-00090-6 (2024).

11 Doll, S. *et al.* ACSL4 dictates ferroptosis sensitivity by shaping cellular lipid composition. *Nat Chem Biol* **13**, 91-98, doi:10.1038/nchembio.2239 (2017).

12 Fumagalli, D. *et al.* Principles Governing A-to-I RNA Editing in the Breast Cancer Transcriptome. *Cell Rep* **13**, 277-289, doi:10.1016/j.celrep.2015.09.032 (2015).

13 Peng, X. *et al.* A-to-I RNA Editing Contributes to Proteomic Diversity in Cancer. *Cancer Cell* **33**, 817-828 e817, doi:10.1016/j.ccell.2018.03.026 (2018).

14 Kung, C. P. *et al.* Evaluating the therapeutic potential of ADAR1 inhibition for triple-negative breast cancer. *Oncogene* **40**, 189-202, doi:10.1038/s41388-020-01515-5 (2021).

15 Karki, R. *et al.* ADAR1 restricts ZBP1-mediated immune response and PANoptosis to promote tumorigenesis. *Cell Rep* **37**, 109858, doi:10.1016/j.celrep.2021.109858 (2021).

16 Liu, H. *et al.* Tumor-derived IFN triggers chronic pathway agonism and sensitivity to ADAR loss. *Nat Med* **25**, 95-102, doi:10.1038/s41591-018-0302-5 (2019).

17 Ishizuka, J. J. *et al.* Loss of ADAR1 in tumours overcomes resistance to immune checkpoint blockade. *Nature* **565**, 43-48, doi:10.1038/s41586-018-0768-9 (2019).

18 Gannon, H. S. *et al.* Identification of ADAR1 adenosine deaminase dependency in a subset of cancer cells. *Nat Commun* **9**, 5450, doi:10.1038/s41467-018-07824-4 (2018).

19 Zhang, T. *et al.* ADAR1 masks the cancer immunotherapeutic promise of ZBP1-driven necroptosis. *Nature* **606**, 594-602, doi:10.1038/s41586-022-04753-7 (2022).

857 20 Mehdipour, P. *et al.* Epigenetic therapy induces transcription of inverted SINEs and
858 ADAR1 dependency. *Nature* **588**, 169-173, doi:10.1038/s41586-020-2844-1 (2020).
859 21 McGuirk, S., Audet-Delage, Y. & St-Pierre, J. Metabolic Fitness and Plasticity in Cancer
860 Progression. *Trends Cancer* **6**, 49-61, doi:10.1016/j.trecan.2019.11.009 (2020).
861 22 Kung, C. P., Maggi, L. B., Jr. & Weber, J. D. The Role of RNA Editing in Cancer
862 Development and Metabolic Disorders. *Front Endocrinol (Lausanne)* **9**, 762,
863 doi:10.3389/fendo.2018.00762 (2018).
864 23 Yang, C. C. *et al.* ADAR1-mediated 3' UTR editing and expression control of antiapoptosis
865 genes fine-tunes cellular apoptosis response. *Cell Death Dis* **8**, e2833,
866 doi:10.1038/cddis.2017.12 (2017).
867 24 Crews, L. A. *et al.* An RNA editing fingerprint of cancer stem cell reprogramming. *J Transl*
868 *Med* **13**, 52, doi:10.1186/s12967-014-0370-3 (2015).
869 25 Jiang, Q. *et al.* Hyper-Editing of Cell-Cycle Regulatory and Tumor Suppressor RNA
870 Promotes Malignant Progenitor Propagation. *Cancer Cell* **35**, 81-94 e87,
871 doi:10.1016/j.ccell.2018.11.017 (2019).
872 26 Almeric, E. *et al.* 3'UTR RNA editing driven by ADAR1 modulates MDM2 expression in
873 breast cancer cells. *Funct Integr Genomics* **25**, 103, doi:10.1007/s10142-025-01611-3
874 (2025).
875 27 Venkatesh, D. *et al.* MDM2 and MDMX promote ferroptosis by PPARalpha-mediated
876 lipid remodeling. *Genes Dev* **34**, 526-543, doi:10.1101/gad.334219.119 (2020).
877 28 Kung, C. P. & Weber, J. D. It's Getting Complicated-A Fresh Look at p53-MDM2-ARF
878 Triangle in Tumorigenesis and Cancer Therapy. *Front Cell Dev Biol* **10**, 818744,
879 doi:10.3389/fcell.2022.818744 (2022).
880 29 Zhao, L. *et al.* Ferroptosis in cancer and cancer immunotherapy. *Cancer Commun (Lond)*
881 **42**, 88-116, doi:10.1002/cac2.12250 (2022).
882 30 Jennis, M. *et al.* An African-specific polymorphism in the TP53 gene impairs p53 tumor
883 suppressor function in a mouse model. *Genes Dev* **30**, 918-930,
884 doi:10.1101/gad.275891.115 (2016).
885 31 Cancer Genome Atlas, N. Comprehensive molecular portraits of human breast tumours.
886 *Nature* **490**, 61-70, doi:10.1038/nature11412 (2012).
887 32 Liu, J., Kang, R. & Tang, D. Adverse effects of ferroptotic therapy: mechanisms and
888 management. *Trends Cancer* **10**, 417-429, doi:10.1016/j.trecan.2024.01.002 (2024).
889 33 Ma, S., Henson, E. S., Chen, Y. & Gibson, S. B. Ferroptosis is induced following
890 siramesine and lapatinib treatment of breast cancer cells. *Cell Death Dis* **7**, e2307,
891 doi:10.1038/cddis.2016.208 (2016).
892 34 Ostenfeld, M. S. *et al.* Effective tumor cell death by sigma-2 receptor ligand siramesine
893 involves lysosomal leakage and oxidative stress. *Cancer Res* **65**, 8975-8983,
894 doi:10.1158/0008-5472.CAN-05-0269 (2005).
895 35 Gagliardi, M. *et al.* Aldo-keto reductases protect metastatic melanoma from ER stress-
896 independent ferroptosis. *Cell Death Dis* **10**, 902, doi:10.1038/s41419-019-2143-7 (2019).
897 36 Gao, F. *et al.* Regulation of endothelial ferroptosis by SESN1 in atherosclerosis and its
898 related mechanism. *Aging (Albany NY)* **15**, 5052-5065, doi:10.18632/aging.204777 (2023).
899 37 Shi, Y. *et al.* alpha-Mangostin suppresses the de novo lipogenesis and enhances the
900 chemotherapeutic response to gemcitabine in gallbladder carcinoma cells via targeting the
901 AMPK/SREBP1 cascades. *J Cell Mol Med* **24**, 760-771, doi:10.1111/jcmm.14785 (2020).

38 Gilbert, N. C. *et al.* Structural and mechanistic insights into 5-lipoxygenase inhibition by natural products. *Nat Chem Biol* **16**, 783-790, doi:10.1038/s41589-020-0544-7 (2020).
39 Bhatt, V. *et al.* Inhibition of autophagy and MEK promotes ferroptosis in Lkb1-deficient Kras-driven lung tumors. *Cell Death Dis* **14**, 61, doi:10.1038/s41419-023-05592-8 (2023).
40 Yin, J. *et al.* 4EBP1-mediated SLC7A11 protein synthesis restrains ferroptosis triggered by MEK inhibitors in advanced ovarian cancer. *JCI Insight* **9**, doi:10.1172/jci.insight.177857 (2024).
41 Larkin, J. *et al.* Combined vemurafenib and cobimetinib in BRAF-mutated melanoma. *N Engl J Med* **371**, 1867-1876, doi:10.1056/NEJMoa1408868 (2014).
42 Diamond, E. L. *et al.* Efficacy of MEK inhibition in patients with histiocytic neoplasms. *Nature* **567**, 521-524, doi:10.1038/s41586-019-1012-y (2019).
43 Brufsky, A. *et al.* A phase II randomized trial of cobimetinib plus chemotherapy, with or without atezolizumab, as first-line treatment for patients with locally advanced or metastatic triple-negative breast cancer (COLET): primary analysis. *Ann Oncol* **32**, 652-660, doi:10.1016/j.annonc.2021.01.065 (2021).
44 Han, H. S. *et al.* Early-Stage Triple-Negative Breast Cancer Journey: Beginning, End, and Everything in Between. *Am Soc Clin Oncol Educ Book* **43**, e390464, doi:10.1200/EDBK_390464 (2023).
45 Yin, C. *et al.* Loss of ADAR1 induces ferroptosis of breast cancer cells. *Cell Signal* **121**, 111258, doi:10.1016/j.cellsig.2024.111258 (2024).
46 He, D., Niu, C., Bai, R., Chen, N. & Cui, J. ADAR1 Promotes Invasion and Migration and Inhibits Ferroptosis via the FAK/AKT Pathway in Colorectal Cancer. *Mol Carcinog*, doi:10.1002/mc.23818 (2024).
47 Murray, M. B., Leak, L. B., Lee, W. C. & Dixon, S. J. Protocol for detection of ferroptosis in cultured cells. *STAR Protoc* **4**, 102457, doi:10.1016/j.xpro.2023.102457 (2023).
48 Enache, O. M. *et al.* Cas9 activates the p53 pathway and selects for p53-inactivating mutations. *Nat Genet* **52**, 662-668, doi:10.1038/s41588-020-0623-4 (2020).
49 Gnanapradeepan, K. *et al.* The p53 Tumor Suppressor in the Control of Metabolism and Ferroptosis. *Front Endocrinol (Lausanne)* **9**, 124, doi:10.3389/fendo.2018.00124 (2018).
50 Qiu, B. *et al.* Phospholipids with two polyunsaturated fatty acyl tails promote ferroptosis. *Cell* **187**, 1177-1190 e1118, doi:10.1016/j.cell.2024.01.030 (2024).
51 Zhang, Y. *et al.* Metabolic switch regulates lineage plasticity and induces synthetic lethality in triple-negative breast cancer. *Cell Metab* **36**, 193-208 e198, doi:10.1016/j.cmet.2023.12.003 (2024).
52 Mendez Ruiz, S., Chalk, A. M., Goradia, A., Heraud-Farlow, J. & Walkley, C. R. Over-expression of ADAR1 in mice does not initiate or accelerate cancer formation in vivo. *NAR Cancer* **5**, zcad023, doi:10.1093/narcan/zcad023 (2023).
53 Avellino, A. *et al.* An Olive Oil-Based High-Fat Diet Promotes Obesity-Driven Metastasis of Triple-Negative Breast Cancer. *Cancer Res* **85**, 5015-5032, doi:10.1158/0008-5472.CAN-25-0822 (2025).
54 Xie, Y. *et al.* Mammary adipocytes protect triple-negative breast cancer cells from ferroptosis. *J Hematol Oncol* **15**, 72, doi:10.1186/s13045-022-01297-1 (2022).
55 Ackermann, T. *et al.* Breast cancer secretes anti-ferroptotic MUFAs and depends on selenoprotein synthesis for metastasis. *EMBO Mol Med* **16**, 2749-2774, doi:10.1038/s44321-024-00142-x (2024).

947 56 Puente-Cobacho, B. *et al.* De novo lipogenesis protects dormant breast cancer cells from
948 ferroptosis and promotes metastasis. *Redox Biology*, 103480,
949 doi:https://doi.org/10.1016/j.redox.2024.103480 (2024).
950 57 Yang, F. *et al.* Ferroptosis heterogeneity in triple-negative breast cancer reveals an
951 innovative immunotherapy combination strategy. *Cell Metab* **35**, 84-100 e108,
952 doi:10.1016/j.cmet.2022.09.021 (2023).
953 58 Park, V. S. *et al.* Lipid Composition Alters Ferroptosis Sensitivity. *Cancer Res* **85**, 4380-
954 4397, doi:10.1158/0008-5472.CAN-24-4207 (2025).
955 59 Park, S. Y. *et al.* Irreversible HER2 inhibitors overcome resistance to the RSL3 ferroptosis
956 inducer in non-HER2 amplified luminal breast cancer. *Cell Death Dis* **14**, 532,
957 doi:10.1038/s41419-023-06042-1 (2023).
958 60 Liu, L. *et al.* ESR1 inhibits ionizing radiation-induced ferroptosis in breast cancer cells via
959 the NEDD4L/CD71 pathway. *Arch Biochem Biophys* **725**, 109299,
960 doi:10.1016/j.abb.2022.109299 (2022).
961 61 Wang, H. *et al.* Strong Protection by 4-Hydroxyestrone against Erastin-Induced Ferroptotic
962 Cell Death in Estrogen Receptor-Negative Human Breast Cancer Cells: Evidence for
963 Protein Disulfide Isomerase as a Mechanistic Target for Protection. *Biochemistry* **63**, 984-
964 999, doi:10.1021/acs.biochem.3c00261 (2024).
965 62 Dibra, D. *et al.* Mutant p53 protects triple-negative breast adenocarcinomas from
966 ferroptosis in vivo. *Sci Adv* **10**, eadk1835, doi:10.1126/sciadv.adk1835 (2024).
967 63 Adams, C. M. *et al.* Targeted MDM2 Degradation Reveals a New Vulnerability for p53-
968 Inactivated Triple-Negative Breast Cancer. *Cancer Discov* **13**, 1210-1229,
969 doi:10.1158/2159-8290.CD-22-1131 (2023).
970 64 Cottrell, K. A., Torres, L. S., Dizon, M. G. & Weber, J. D. 8-azaadenosine and 8-
971 chloroadenosine are not selective inhibitors of ADAR. *Cancer Res Commun* **1**, 56-64,
972 doi:10.1158/2767-9764.crc-21-0027 (2021).
973 65 Rehwinkel, J. & Mehdipour, P. ADAR1: from basic mechanisms to inhibitors. *Trends Cell*
974 *Biol*, doi:10.1016/j.tcb.2024.06.006 (2024).
975 66 Weth, F. R. *et al.* Unlocking hidden potential: advancements, approaches, and obstacles in
976 repurposing drugs for cancer therapy. *Br J Cancer* **130**, 703-715, doi:10.1038/s41416-023-
977 02502-9 (2024).
978 67 Lee, J. *et al.* Anti-tumor and anti-metastasis efficacy of E6201, a MEK1 inhibitor, in
979 preclinical models of triple-negative breast cancer. *Breast Cancer Res Treat* **175**, 339-351,
980 doi:10.1007/s10549-019-05166-3 (2019).
981 68 Lulli, D., Carbone, M. L. & Pastore, S. The MEK Inhibitors Trametinib and Cobimetinib
982 Induce a Type I Interferon Response in Human Keratinocytes. *Int J Mol Sci* **18**,
983 doi:10.3390/ijms18102227 (2017).
984 69 Deng, J. *et al.* Targeting Cancer Cell Ferroptosis to Reverse Immune Checkpoint Inhibitor
985 Therapy Resistance. *Front Cell Dev Biol* **10**, 818453, doi:10.3389/fcell.2022.818453
986 (2022).
987 70 Martinez-Garay, C. & Djouder, N. Dietary interventions and precision nutrition in cancer
988 therapy. *Trends Mol Med* **29**, 489-511, doi:10.1016/j.molmed.2023.04.004 (2023).

989

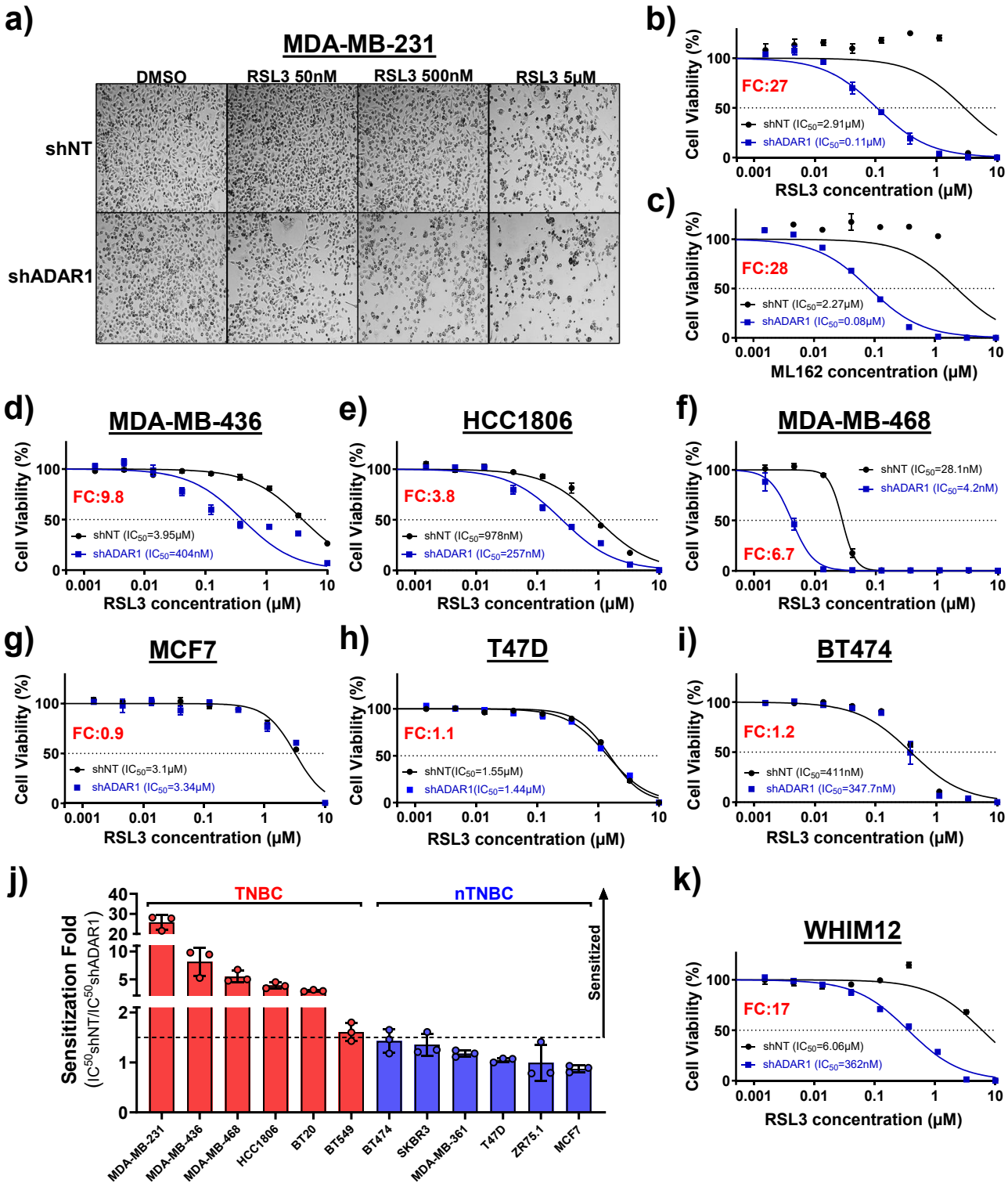
a)
MDA-MB-231
DMSO
RSL3 50nM
RSL3 500nM
RSL3 5μM
shNT
shADAR1
b)
Cell Viability (%)
FC:27
shNT (IC50=2.91μM)
shADAR1 (IC50=0.11μM)
RSL3 concentration (μM)
c)
FC:28
shNT (IC50=2.27μM)
shADAR1 (IC50=0.08μM)
ML162 concentration (μM)
d)
MDA-MB-436
FC:9.8
shNT (IC50=3.95μM)
shADAR1 (IC50=404nM)
e)
HCC1806
FC:3.8
shNT (IC50=978nM)
shADAR1 (IC50=257nM)
f)
MDA-MB-468
FC:6.7
shNT (IC50=28.1nM)
shADAR1 (IC50=4.2nM)
g)
MCF7
FC:0.9
shNT (IC50=3.1μM)
shADAR1 (IC50=3.34μM)
h)
T47D
FC:1.1
shNT(IC50=1.55μM)
shADAR1(IC50=1.44μM)
i)
BT474
FC:1.2
shNT (IC50=411nM)
shADAR1 (IC50=347.7nM)
j)
TNBC
nTNBC
Sensitization Fold
(IC50shNT/IC50shADAR1)
Sensitized
MDA-MB-231
MDA-MB-436
MDA-MB-468
HCC1806
BT20
BT549
BT474
SKBR3
MDA-MB-361
T47D
ZR75.1
MCF7
k)
WHIM12
FC:17
shNT (IC50=6.06μM)
shADAR1 (IC50=362nM)

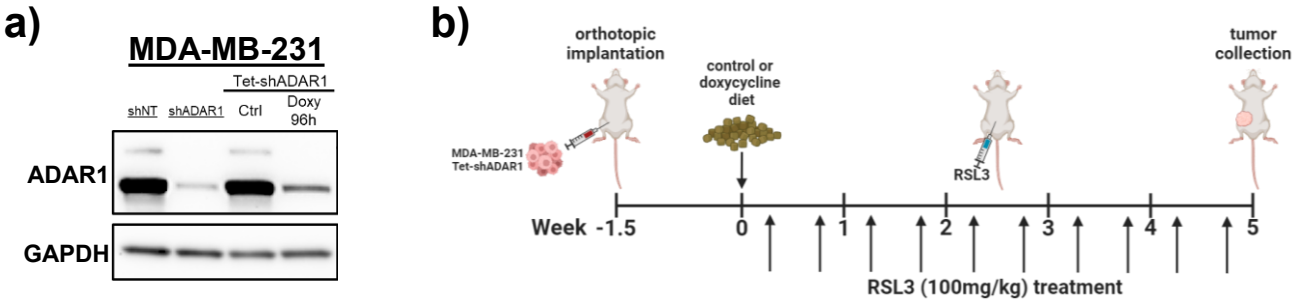

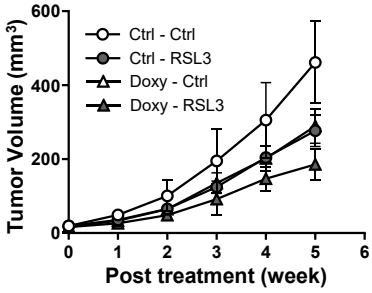

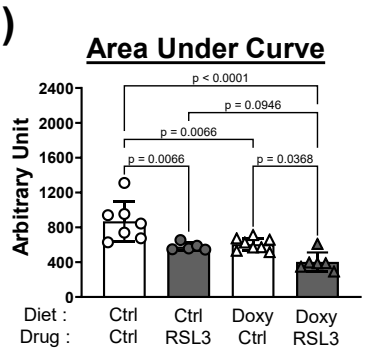

e)

Comparison		p-Value - Post Treatment (Week)					
Group 1	Group 2	0	1	2	3	4	5
Ctrl - Ctrl	Doxy - Ctrl	>0.999	0.957	0.367	0.015	<0.0001	<0.0001
Ctrl - Ctrl	Ctrl - RSL3	>0.999	0.984	0.472	0.005	<0.0001	<0.0001
Ctrl - Ctrl	Doxy - RSL3	>0.999	0.836	0.087	<0.0001	<0.0001	<0.0001
Doxy - Ctrl	Doxy - RSL3	>0.999	0.999	0.963	0.234	0.059	<0.0001
Ctrl - RSL3	Doxy - RSL3	>0.999	0.997	0.964	0.606	0.120	0.002

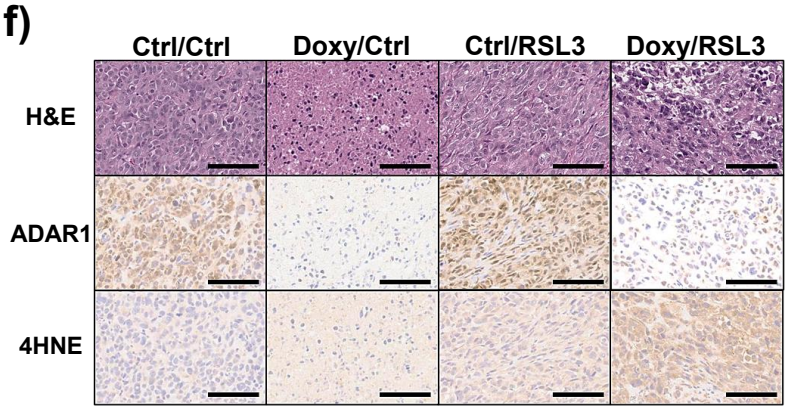

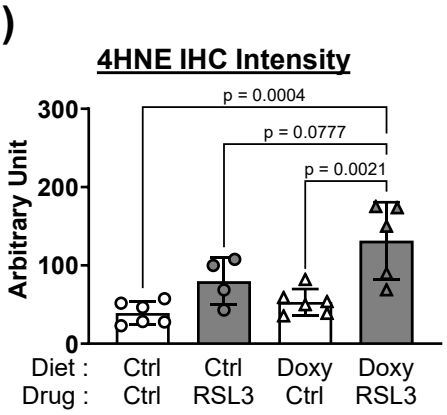

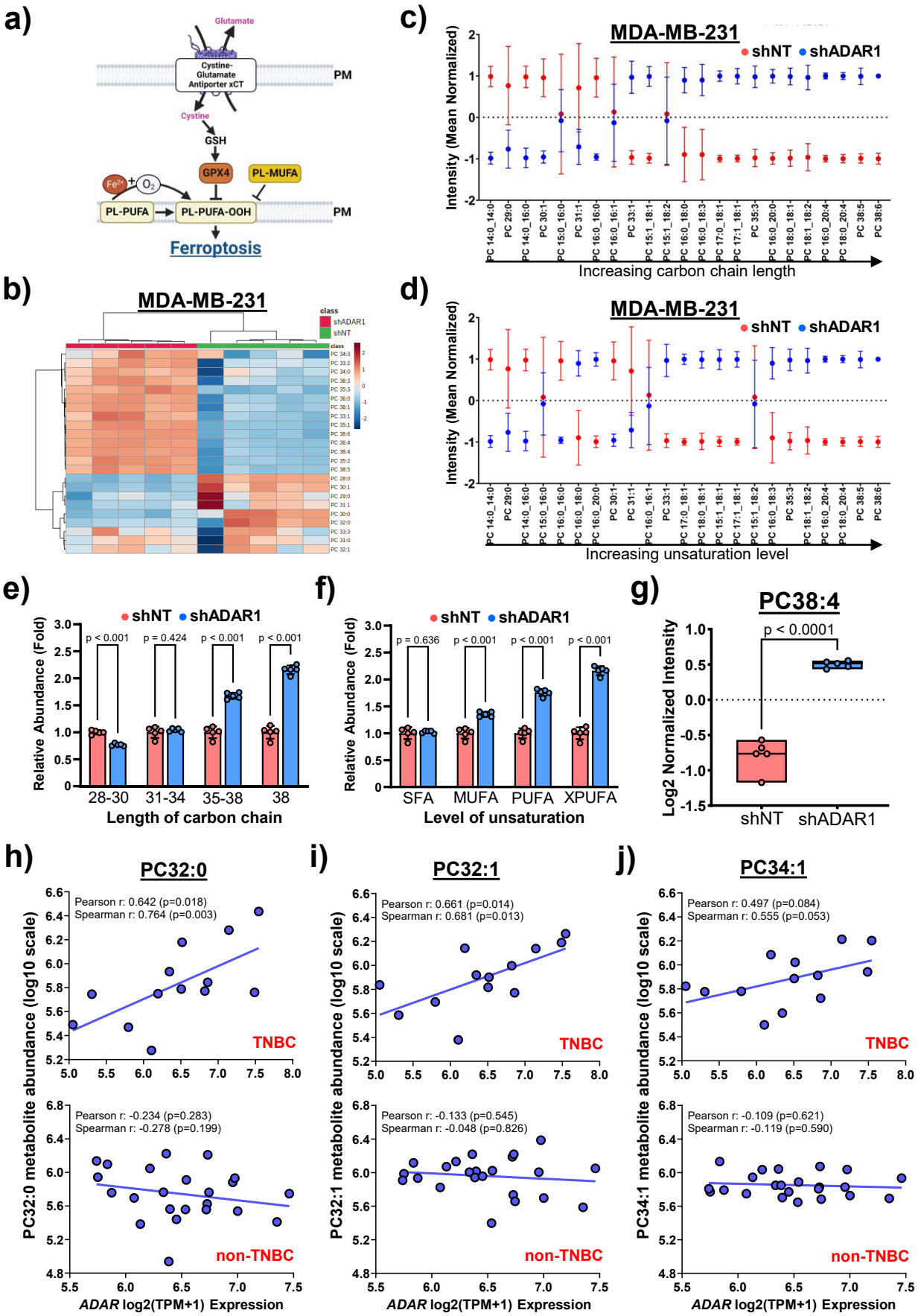
a)
Glutamate
Cystine-Glutamate Antiporter xCT
PM
Cystine
GSH
GPX4
PL-MUFA
PL-PUFA
PL-PUFA-OOH
PM
Ferroptosis
b)
MDA-MB-231
class
shADAR1
shNT
c)
MDA-MB-231
shNT
shADAR1
Intensity (Mean Normalized)
Increasing carbon chain length
d)
MDA-MB-231
shNT
shADAR1
Intensity (Mean Normalized)
Increasing unsaturation level
e)
shNT
shADAR1
Relative Abundance (Fold)
p < 0.001
p = 0.424
p < 0.001
p < 0.001
28-30
31-34
35-38
38
Length of carbon chain
f)
shNT
shADAR1
Relative Abundance (Fold)
p = 0.636
p < 0.001
p < 0.001
p < 0.001
SFA
MUFA
PUFA
XPUFA
Level of unsaturation
g)
PC38:4
p < 0.0001
Log2 Normalized Intensity
shNT
shADAR1
h)
PC32:0
Pearson r: 0.642 (p=0.018)
Spearman r: 0.764 (p=0.003)
TNBC
Pearson r: -0.234 (p=0.283)
Spearman r: -0.278 (p=0.199)
non-TNBC
PC32:0 metabolite abundance (log10 scale)
ADAR log2(TPM+1) Expression
i)
PC32:1
Pearson r: 0.661 (p=0.014)
Spearman r: 0.681 (p=0.013)
TNBC
Pearson r: -0.133 (p=0.545)
Spearman r: -0.048 (p=0.826)
non-TNBC
PC32:1 metabolite abundance (log10 scale)
ADAR log2(TPM+1) Expression
j)
PC34:1
Pearson r: 0.497 (p=0.084)
Spearman r: 0.555 (p=0.053)
TNBC
Pearson r: -0.109 (p=0.621)
Spearman r: -0.119 (p=0.590)
non-TNBC
PC34:1 metabolite abundance (log10 scale)
ADAR log2(TPM+1) Expression

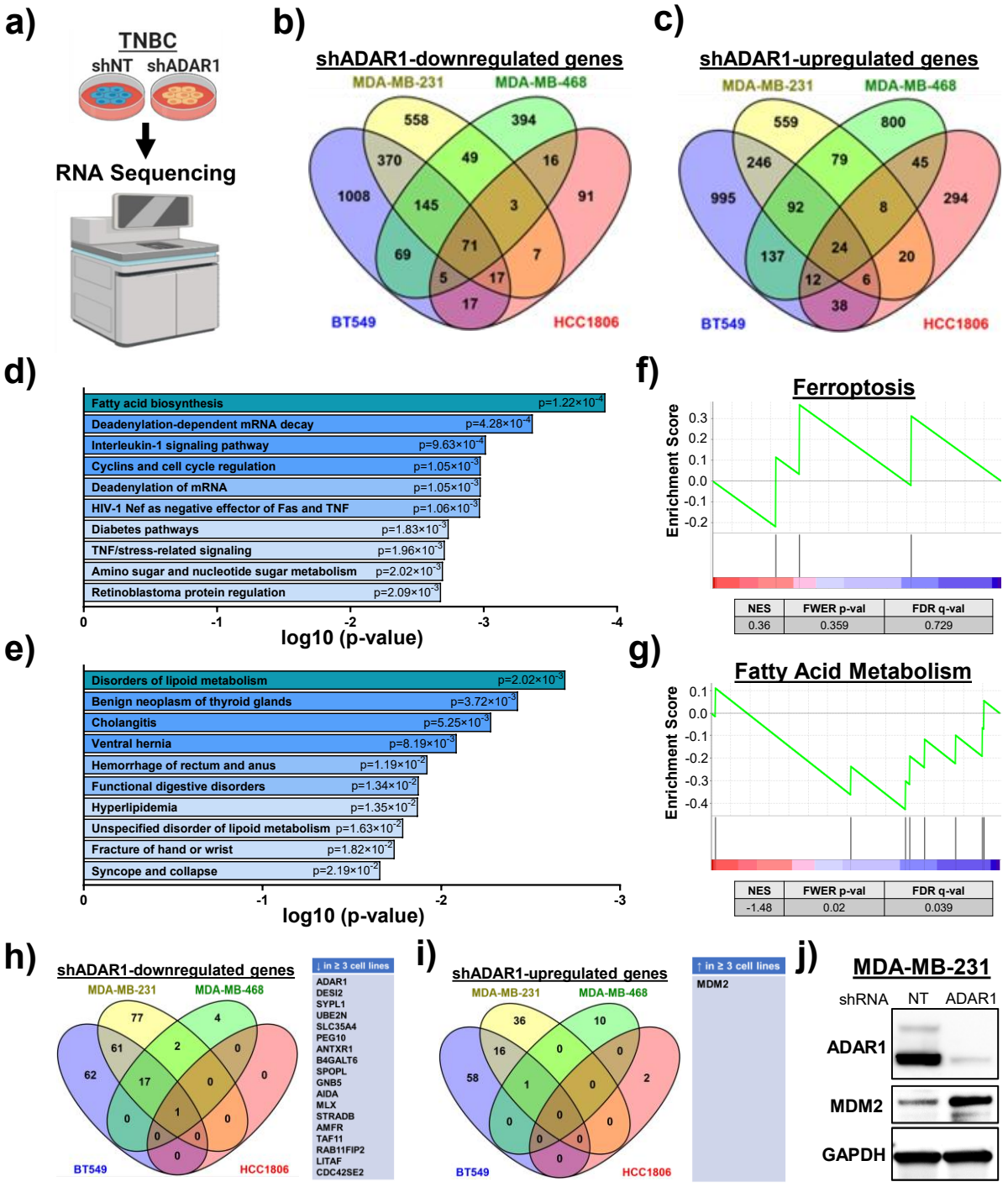
a)
TNBC
shNT shADAR1
RNA Sequencing
b)
shADAR1-downregulated genes
MDA-MB-231
MDA-MB-468
BT549
HCC1806
558
394
370
49
16
1008
145
3
91
69
71
7
5
17
17
c)
shADAR1-upregulated genes
MDA-MB-231
MDA-MB-468
BT549
HCC1806
559
800
246
79
45
995
92
8
294
137
24
20
12
6
38
d)
Fatty acid biosynthesis p=1.22×10-4
Deadenylation-dependent mRNA decay p=4.28×10-4
Interleukin-1 signaling pathway p=9.63×10-4
Cyclins and cell cycle regulation p=1.05×10-3
Deadenylation of mRNA p=1.05×10-3
HIV-1 Nef as negative effector of Fas and TNF p=1.06×10-3
Diabetes pathways p=1.83×10-3
TNF/stress-related signaling p=1.96×10-3
Amino sugar and nucleotide sugar metabolism p=2.02×10-3
Retinoblastoma protein regulation p=2.09×10-3
0 -1 -2 -3 -4
log10 (p-value)
e)
Disorders of lipoid metabolism p=2.02×10-3
Benign neoplasm of thyroid glands p=3.72×10-3
Cholangitis p=5.25×10-3
Ventral hernia p=8.19×10-3
Hemorrhage of rectum and anus p=1.19×10-2
Functional digestive disorders p=1.34×10-2
Hyperlipidemia p=1.35×10-2
Unspecified disorder of lipoid metabolism p=1.63×10-2
Fracture of hand or wrist p=1.82×10-2
Syncope and collapse p=2.19×10-2
0 -1 -2 -3
log10 (p-value)
f)
Ferroptosis
Enrichment Score
0.3 0.2 0.1 0.0 -0.1 -0.2
NES | FWER p-val | FDR q-val
0.36 | 0.359 | 0.729
g)
Fatty Acid Metabolism
Enrichment Score
0.1 0.0 -0.1 -0.2 -0.3 -0.4
NES | FWER p-val | FDR q-val
-1.48 | 0.02 | 0.039
h)
shADAR1-downregulated genes
MDA-MB-231
MDA-MB-468
BT549
HCC1806
77
4
61
2
0
62
17
0
0
1
0
0
0
0
0
↓ in ≥ 3 cell lines
ADAR1
DESI2
SYPL1
UBE2N
SLC35A4
PEG10
ANTXR1
B4GALT6
SPOPL
GNB5
AIDA
MLX
STRADB
AMFR
TAF11
RAB11FIP2
LITAF
CDC42SE2
i)
shADAR1-upregulated genes
MDA-MB-231
MDA-MB-468
BT549
HCC1806
36
10
16
0
0
58
1
0
2
0
0
0
0
0
0
↑ in ≥ 3 cell lines
MDM2
j)
MDA-MB-231
shRNA NT ADAR1
ADAR1
MDM2
GAPDH

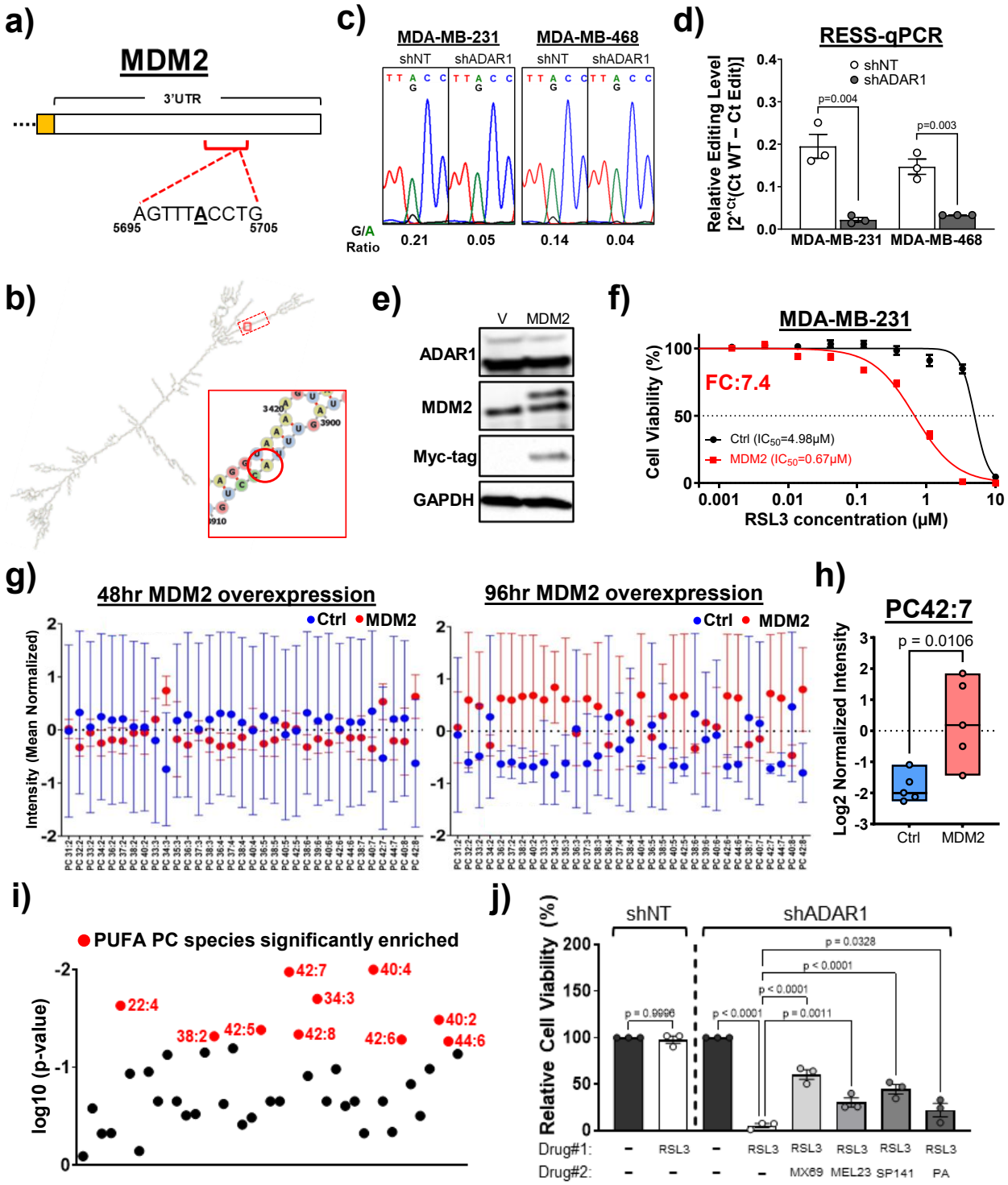
a)
MDM2
3'UTR
AGTTTACCTG
5695
5705
c)
MDA-MB-231
MDA-MB-468
shNT
shADAR1
G/A Ratio
0.21
0.05
0.14
0.04
d)
RESS-qPCR
shNT
shADAR1
Relative Editing Level [2^-Ct(Ct WT – Ct Edit)]
p=0.004
p=0.003
MDA-MB-231
MDA-MB-468
b)
e)
V
MDM2
ADAR1
MDM2
Myc-tag
GAPDH
f)
MDA-MB-231
FC:7.4
Cell Viability (%)
Ctrl (IC50=4.98μM)
MDM2 (IC50=0.67μM)
RSL3 concentration (μM)
g)
48hr MDM2 overexpression
96hr MDM2 overexpression
Ctrl
MDM2
Intensity (Mean Normalized)
h)
PC42:7
p = 0.0106
Log2 Normalized Intensity
Ctrl
MDM2
i)
PUFA PC species significantly enriched
log10 (p-value)
22:4
38:2
42:5
42:7
42:8
34:3
40:4
42:6
40:2
44:6
j)
shNT
shADAR1
Relative Cell Viability (%)
p = 0.9996
p < 0.0001
p < 0.0001
p = 0.0011
p < 0.0001
p = 0.0328
Drug#1:
Drug#2:
RSL3
MX69
MEL23
SP141
PA

a)

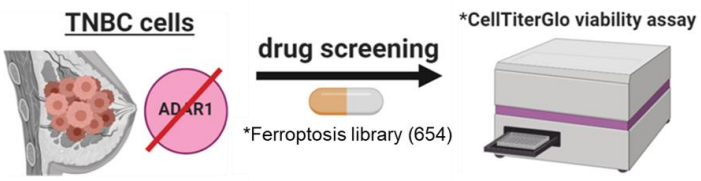

b)

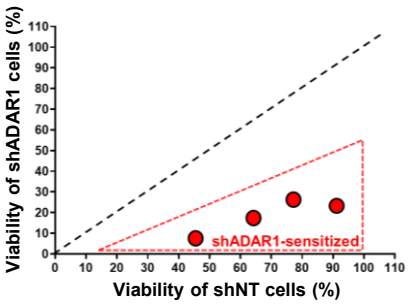

c)

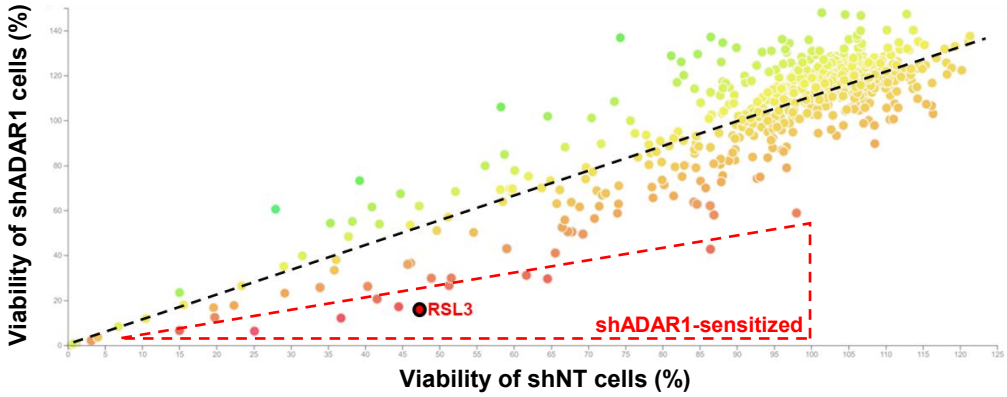

d)

Drug	Viability Ratio (shADAR1/shNT)
Siramesine	0.26
SB-590885	0.33
α-Mangostin	0.39
GW284543	0.45
UC2288	0.46
Nordihydroguaiaretic acid (NDGA)	0.5
Cobimetinib	0.51
Cobimetinib (racemate)	0.51

e)

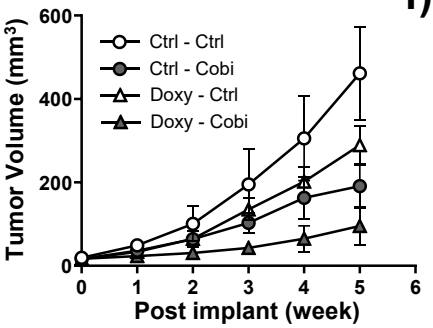

f)

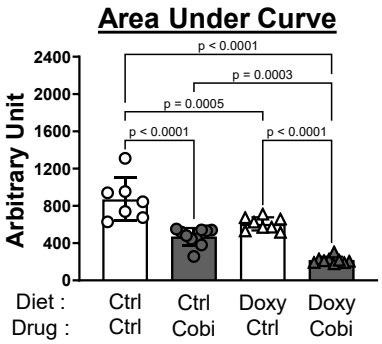

g)

Comparison		p-Value - Post Treatment (Week)					
Group 1	Group 2	0	1	2	3	4	5
Ctrl - Ctrl	Doxy - Ctrl	>0.999	0.957	0.367	0.015	<0.0001	<0.0001
Ctrl - Ctrl	Ctrl - Cobi	>0.999	0.979	0.319	<0.0001	<0.0001	<0.0001
Ctrl - Ctrl	Doxy - Cobi	>0.999	0.725	0.002	<0.0001	<0.0001	<0.0001
Doxy - Ctrl	Doxy - Cobi	>0.999	0.994	0.436	<0.0001	<0.0001	<0.0001
Ctrl - Cobi	Doxy - Cobi	>0.999	0.980	0.426	0.011	<0.0001	<0.0001
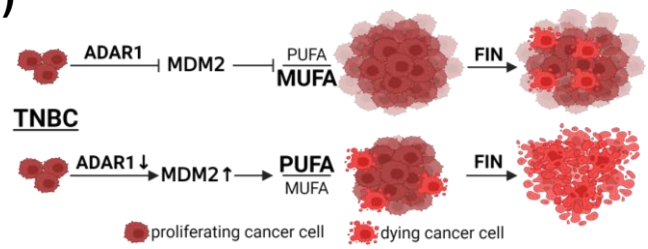
h)